IN-SITU MONITORING OF PHOTOPOLYMERIZATION USING MICRORHEOLOGY

A Thesis

Presented to

The Academic Faculty

By

Ryan Patrick Slopek

In Partial Fulfillment

of the Requirements for the Degree

Master of Science in Chemical and Biomolecular Engineering

Georgia Institute of Technology

August 2005

IN-SITU MONITORING OF PHOTOPOLYMERIZATION USING MICRORHEOLOGY

APPROVED BY:

Dr. Victor Breedveld, Thesis Chair
School of Chemical and Biomolecular Engineering
Georgia Institute of Technology

Dr. Cliff Henderson
School of Chemical and Biomolecular Engineering
Georgia Institute of Technology

Dr. Pete Ludovice
School of Chemical and Biomolecular Engineering
Georgia Institute of Technology

Date Approved: July 6, 2005

ACKNOWLEDGEMENTS

First and foremost, I would to thank my research advisor, Dr. Victor Breedveld, for his guidance, insight, patience, and time. His encouragement and advice greatly contributed to the success of this research. I would also like to thank Dr. Cliff Henderson for sharing his knowledge of photo-induced curing and for allowing me the use of several key pieces of research equipment. In addition, I would like to thank Dr. Pete Ludovice for taking the time and agreeing to be a part of my committee.

I am also eternally grateful to many others for directly helping with this research. Specifically, I would like to thank Haris McKinley for the time and knowledge he invested in starting this research project. I am grateful to Yanyan Tang, for answering my questions and allowing me the opportunity to compare my experimental results to her modeled results. I would also like to thank Rebecca Shiels for providing the time, knowledge, and equipment necessary to accomplish the deoxygenation portion of this research. I will forever be indebted to both Dr. Raymond Tu and Jun Sato for the countless times they helped out along the way.

I would like to thank my friends for making the best of the worst times—thank you all so much. I am especially grateful Akua, Ayanna, and Krista, who stuck with me in good times and bad—you'll always remain in my thoughts and prayers. Finally, I would like to thank my parents for their unbounded support and encouragement—words cannot thank you enough.

TABLE OF CONTENTS

Section Title	Page Number
ACKNOWLEDGEMENTS	**iii**
LIST OF TABLES	**vii**
LIST OF FIGURES	**viii**
SUMMARY	**xi**
CHAPTER 1 INTRODUCTION	**1**
1.1 Overview	1
1.2 Past Research	2
1.3 Project Overview	6
1.4 Project Approach	7
1.5 Thesis Outline	8
CHAPTER 2 PHOTOPOLYMERIZATION	**9**
2.1 Photopolymerization Overview	9
2.2 Free-Radical Photoresins	11
2.2.1 Acrylate and Methacrylate Systems	12
2.2.2 Thiol-Ene Systems	13
2.2.3 Unsaturated Polyesters	14
2.3 Photoinitiators	14
2.3.1 Unimolecular Photoinitiators (Type I)	15
2.3.2 Bimolecular Photoinitiator Systems (Type II)	16

2.3.3 Photosensitizes 17

2.4 Kinetics 18

2.4.1 Initiation 19
2.4.2 Propagation 21
2.4.3 Termination 22
2.4.4 Inhibition 22
2.4.5 Summary of Basic Kinetic Equations 24

2.5 Gelation Theory 25

2.6 Applications 28

2.6.1 Film, Coatings, and Adhesives 29
2.6.2 Biomaterials 29
2.6.3 Stereolithography 30

CHAPTER 3 MICRORHEOLOGY 32

3.1 Overview of Microrheology 32

3.2 Theory of Particle Tracking Microrheology 33

3.3 Techniques Used to Study Photopolymerization 36

3.3.1 Spectroscopy 36
3.3.2 Calorimetry 38
3.3.3 Rheology 38

CHAPTER 4 EXPERIMENTAL 42

4.1 Photopolymerization System 42

4.1.1 Monomer 42
4.1.2 Photoinitiator 44
4.1.3 Fluorescent Tracer Particles 46
4.1.4 Sample Preparation 46

4.2 Experimental Design 47

4.2.1 Fabrication of Sample Chamber 47
4.2.2 Experimental Setup 49
4.2.3 Data Acquisition 51

4.2.4 System Parameters 52

4.2.4.1 Wavelength of UV Light 53
4.2.4.2 Intensity of UV Light 53
4.2.4.3 Location in Sample 55
4.2.4.4 Addition of Inhibitor 56
4.2.4.5 Deoxygenation 57

4.3 Analytical Procedure 57

4.3.1 IDL 58
4.3.2 Definition of Gel Point with Microrheology 59

CHAPTER 5 RESULTS AND DISCUSSION 61

5.1 Proof of Concept Results 61

5.2 Depth Profiling 67

5.3 Intensity Effects and Beer's Law 73

5.4 Kinetic Effects 79

5.4.1 Concentration of Inhibitor 79
5.4.2 Concentration of Photoinitiator and Oxygen Inhibition 81

CHAPTER 6 CONCLUSIONS AND RECOMMENDATIONS 87

6.1 Summary of Results 87

6.2 Conclusions 88

6.3 Recommendations 89

6.4 Future Research 92

REFERENCES 96

LIST OF TABLES

Table		Page Number
Table 4.1	Informational summary of acrylate monomers used in this investigation.	44
Table 4.2	Measured intensity of UV light at 248 nm and 356 nm using filters with various optical densities.	55

LIST OF FIGURES

Figure		Page Number
Figure 2.1	Molecular structure of a generalized acrylate monomer and its corresponding polymer repeat unit.	12
Figure 2.2	Generalized reaction scheme for an unsaturated polyester system.	14
Figure 2.3	Cleavage mechanism of unimolecular photoinitiator free-radical generation.	16
Figure 2.4	Hydrogen abstraction mechanism of unimolecular photoinitiator free-radical generation between the photoinitiator benzophenone and the hydrogen donor tetrahydrofuran.	16
Figure 2.5	General bimolecular photoinitiator free-radical generation mechanism shown for intramoleculer H-abstraction of photoinitiator 1-phyenyl-butan-1-one.	16
Figure 2.6	Schematic representation of linear photopolymerization kinetics.	18
Figure 2.7	Schematic representation of the kinetics of a multifunctional photopolymerization reaction.	19
Figure 2.8	Steady shear viscosity and equilibrium modulus of a crossing-linking polymer as a function of reaction time.	26
Figure 2.9	Process of stereolithography.	31
Figure 3.1	Principles of particle tracking microrheology: from particle motion to sample rheology.	34
Figure 4.1	Absorption Spectra of Ciba Irgacure 651 at different concentrations in acetonitrile.	45

Figure 4.2	Schematic of fabricated sample chamber loaded with a sample.	48
Figure 4.3	Transmission spectrum of glass cover slip and microscope slide.	49
Figure 4.4	Spectral irradiance of 1000 W Hg(Xe) arc lamp.	50
Figure 4.5	Schematic of the experimental setup.	51
Figure 4.6	Schematic of data acquisition and experimental setup.	52
Figure 4.7	Transmission spectrum of 248nm UV bandpass filter and 356 nm UV bandpass filter.	53
Figure 4.8	Picture of neutral density filters.	54
Figure 4.9	Transmission spectrum of ND01, ND03, and ND10 neutral density filters.	55
Figure 4.10	Illustration of sample depth.	56
Figure 5.1	MSD of tracer particles as a function of lag time for SR494 with 5.0 wt% photoinitiator.	61
Figure 5.2	Transient MSD for tracer particles in a curing sample of SR494 loaded with 5.0 wt% photoinitiator. The inset illustrates how the corresponding figure can be interpreted in terms of gels and liquids. Gelation occurs at image number 590.	62
Figure 5.3	Graph of slope value vs. image number. The data was fitted to a sigmoidal curve. Gel point occurs when slope is equal to 0.5 (i.e., approximately at image number 592).	64
Figure 5.4	Spatial variations of tracer particle MSD in a partly exposed cured sample of SR351 loaded with 1.0 wt% photoinitiator.	66
Figure 5.5	Plot of gelation time as a function of UV penetration depth for SR494 loaded with 5.0 wt% photoinitiator cured using both 248 nm and 356 nm UV irradiation.	68

Figure 5.6	Plot of gelation time as a function of UV penetration depth for three different acrylate monomers: SR272, SR351, and SR494. All samples were loaded with 5.0 wt% photoinitiator and cured using 356 nm UV irradiation.	70
Figure 5.7	Plot of gelation time as a function of UV penetration depth and Intensity for SR494 loaded with 5.0 wt% photoinitiator cured using 248 nm UV irradiance.	71
Figure 5.8	Plot of gelation time as a function of UV penetration depth and Intensity for SR494 loaded with 5.0 wt% photoinitiator cured using 356 nm UV irradiance.	72
Figure 5.9	Plot of gelation time normalized to the unfiltered UV intensity as a function of UV penetration depth and Intensity for SR494 loaded with 5.0 wt% photoinitiator cured using 248 nm UV irradiance.	75
Figure 5.10	Plot of gelation time normalized to the unfiltered UV intensity as a function of UV penetration depth and Intensity for SR494 loaded with 5.0 wt% photoinitiator cured using 356 nm UV irradiance.	75
Figure 5.11	Plot of gelation time as a function of inhibitor (MEHQ) concentration for SR494 loaded with 5.0 wt% photoinitiator cured using 356 nm UV irradiance. The vertical line indicates the concentration of inhibitor sample as received (240 ppm MEHQ).	78
Figure 5.12	Plot of gelation time as a function of initiator (Irgacure 651) loading concentration for both oxygenated and degassed samples of SR494 cured using 356 nm UV irradiance. Plotted in: A: a linear scale, B: linear, and C: double logarithmic scale.	80
Figure 6.1	Experimental design for spatial patterned photo-masks.	91
Figure 6.2	Temporal modulation of illumination profile using electronic shutters.	91

SUMMARY

Photopolymerization is the basis of several multi-million dollar industries including films and coating, inks, adhesives, fiber optics, and biomaterials. The fundamentals of the photopolymerization process, however, are not well understood. As a result, spatial variations of photopolymerization impose significant limitations on applications in which a high spatial resolution is required.

To address these issues, microrheology was implemented to study the spatial and temporal effects of free-radical photopolymerization. In this work a photosensitive, acrylate resin was exposed to ultraviolet light, while the Brownian motion of micron sized, inert fluorescent tracer particles was tracked using optical videomicroscopy. Statistical analysis of particle motion yielded data that could then be used to extract rheological information about the embedding medium as a function of time and space, thereby relating UV exposure to the polymerization and gelation of monomeric resins.

The effects of varying depth, initiator concentration, inhibitor concentration, composition of the monomer, and light intensity on the gelation process were studied. The most striking result is the measured difference in gelation time observed as a function of UV penetration depth. The observed trend was found to be independent of UV light intensity and monomer composition. The intensity results were used to test the accuracy of energy threshold model, which is used to empirically predict photo-induced polymerization.

The results of this research affirm the ability of microrheology to provide the high spatial and temporal resolution necessary to accurately monitor the photopolymerization process. The experimental data provide a better understanding of the photo-induced polymerization, which could lead to expanded use and improved industrial process optimization. The use of microrheology to monitor photopolymerization can also aid in the development of predictive models and offer the ability to perform in-situ quality control of the process.

CHAPTER 1

INTRODUCTION

In this chapter, the importance of photopolymerization to both industry and the consumer will be stressed, along with the current issues that limit the application of photopolymerization. In addition, a brief review of research performed in the area will be offered. The goals of this research project will then be formulated to investigate and resolve some of the present limitations of photopolymerization.

1.1. Overview

Photopolymerization is the basis of several multi-million dollar industries. UV-initiated photopolymerization of multifunctional monomers in the presence of a photoinitiator is one of the most efficient methods to produce solid coatings and objects from polymeric materials. The process results in the almost instantaneous transformation of a liquid resin into a highly cross-linked solid polymer that is totally insoluble in organic solvents and very resistant to both heat and mechanical treatments. Several books[1-4] and reviews[5-6] have been written on the subject of photopolymerization.

Besides the high cure speed, light-induced polymerization has a number of other favorable features such as solvent-free formulation, low energy consumption, ambient temperature operation, and high quality as well as tunable properties like color, flexibility, clarity, and surface characteristics of the final products. Because of its distinct

advantages, this technology has experienced a steady growth over the last few decades. UV-curing has become an established technology for a large variety of commercial applications, primarily in the coating and printing industries, but also in photolithography, biomaterials, the manufacture of adhesives, and restorative dental materials.

A number of drawbacks in photopolymerization, however, have limited its use in some applications. Inhibition by oxygen in free-radical polymerization and by water vapor in cationic polymerization leads to a significant decrease in cure speed and overall quality of the final product. Another disadvantage is the inability of many lasers and UV exposure tools to homogeneously cure thick or strongly absorbing systems. Furthermore, the problem of shrinkage during polymerization negatively affects applications that require accurate part shape and size. Health and safety concerns about the toxicity of some commonly used photoresins are additional complications that must be addressed within industrial applications. In general, intricate applications of photopolymerization such as optical, medical, and electronic materials, demand a more complete understanding of the evolution of mechanical properties.

1.2. Past Research

Techniques that allow the measurement of chemical and mechanical changes in real-time or pseudo real-time have gained recent significance in the prospect of improving control over the development of mechanical properties during photopolymerization. The first time-resolved techniques used to monitor photopolymerization were spectroscopic (IR and Raman) and photo-DSC[7]. Photo-DSC,

which measures the flow of exothermic heat released from the conversion of a carbon double bond, was found to have the drawbacks of long response time due to sample thermal conductivity[8]. Spectroscopic time-resolved research was further improved with the development of Fourier transform instruments that allowed multiple peak monitoring of different chemical reactive groups[9]. Time-resolved spectroscopy of photopolymerization reactions has also been extended to near IR[10] and Raman spectroscopy[11]; however, spectroscopic techniques focus on chemical changes within the resin and do not provide information about the development of mechanical properties.

Rolla *et al.* used microwave dielectric measurements to examine the cross-linking polymerization of mono-functional *n*-butyl acrylate[12] as well as blends of difunctional hexane and diol diacrylate that produce dense cross-linked networks[13]. The researchers monitored the decreasing acrylate monomer concentration via a linear correlation with the dielectric loss index at microwave frequencies. This allowed for one of the first detailed studies of the reaction kinetics of acrylate systems[12, 13].

Direct time-resolved measurement of mechanical properties was first developed independently by Nakamuchi and Watanabe *et al.* using an oscillating plate rheometer fitted with a quartz parallel plate system[14, 15]. The researchers used changes in the phase angle to determine that the dynamic viscosity of a photopolymer increased upon exposure to UV light. The parallel plate setup had an increased risk of the two plates grinding against each other when shrinkage occurred. Guthrie *et al.* developed a cone and plate geometry with a modified quartz plate to monitor cationic and free-radical photopolymerizations[16].

Khan *et al.* developed a technique that allowed for the transient measurement of the mechanical properties of a photoresin. Using a rheometer fitted with quartz glass plates, Khan and co-workers were able to measure the evolution of rheological mechanical properties in a temperature-controlled cell[17]. This technique was used to monitor thiol-ene step growth cross-linking photopolymerization. The combination of UV illumination with a rheometer made it possible to monitor rheological properties at several frequencies, which enabled Khan and his co-workers to apply the well-known Winter—Chambon criteria for gelation and show that the loss tangent becomes independent of frequency at the gel point. The researchers demonstrated that the cross-linking rate of thiol-ene increases when increasing the monomer functionality or the temperature.

In an attempt to further the understanding of the relationship between thiol conversion and mechanical properties, Khan *et al.* performed separate Fourier transform infrared spectroscopy (FTIR) and rheological experiments using the same light intensity and film thickness[18]. FTIR studies revealed that the thiol-ene polymerization follows a second order polymerization until about 70% conversion. Real-time rheological measurements under identical UV illumination conditions revealed that the modulus did not change significantly until 65% thiol conversion. Comparable gel times were found from both FTIR and real-time rheology analysis.

Fourier transform infrared attenuated total reflectance (FTIR-ATR) was used by Scherzer and Dietz *et al.* to study the radical photopolymerization reactions of various acrylate systems[19, 20]. The FTIR-ATR technique permits the sample layer to be studied horizontally as opposed to vertically in most FTIR setups. FTIR-ATR has the advantage

of being able to measure low viscosity samples that can not be measured with standard FTIR. Scherzer found that temperature had a strong effect on the kinetics of photopolymerization. In the same work, Scherzer showed that aliphatic acrylates could be photopolymerized in the absence of photoinitiator simply by exposure to short-wavelength monochromatic UV light. Dietz and co-workers found that by varying the film thickness of the sample, kinetic parameters of multiacrylates could be determined as a function of space.

Lange and Naghash have used the technique developed by Khan and co-workers to determine the viscoelastic properties during UV curing of methacrylate-based resins[21, 22]. Lange compared transitions during thermal and UV curing and found that the method of cure influences the physical properties of the final cured material. Claesson *et al.* used the Khan technique to measure the viscoelastic behavior during ultra-fast star-branched polymerization[23]. Claesson and co-workers found that the time to reach the gel point increases linearly with molecular weight of the monomer. Botella *et al.* took Khan's idea of individually measuring FTIR and rheology one step further when they combined the techniques into one method[24]. The researchers used the technique to study the conversion and viscoelastic properties of a dimethacrylate/styrene based system. It was found that a lower illumination intensity delays the reaction but the viscoelastic properties are purely a function of conversion, not conversion rate.

Lee and co-workers used a stereolithography apparatus to examine cure depth as a function of photoinitiator concentration and laser dosage in the photopolymerization of 2,2-bis{4-[2-hydroxy-3-(methacryloxy)propoxy]phenyl}-propane (Bis-GMA)[25]. They observed that the concentration of photoinitiator plays a key role in controlling the

quality and performance of the formed gel network, especially with regards to the thickness of cured layers. In addition, they determined that shrinkage could be reduced by minimizing the ratio of swelling that observed when a cross-linked polymer is placed in a solvent. The researchers developed a model capable of predicting the optimal photoinitiator concentration and the corresponding cure depth, while minimizing overall shrinkage of the system. The model incorporates reaction kinetics, but the phenomena of oxygen quenching of radicals and polymerization autoacceleration are not included.

1.3. Project Objective

As stated above, photopolymerization is the basis of many applications; however, several limitations that result from a general lack of understanding about the process continue to plague the industry. Specifically, spatial variations of photopolymerization impose significant limitations on applications in which a high spatial resolution is required such as rapid prototyping. Rapid prototyping is used to create scale models; and therefore, excellent control of part shape and size is critical. The experimental ability to examine and quantify product inhomogeneity caused by spatial variations in photopolymerization systems would be of great benefit to industry. This information could ultimately be used to strengthen and validate curing models that are currently used to control and predict the process of photopolymerization.

The steady evolution of UV curing technology has created a need for the development of experimental methods that allow monitoring of photopolymerization reactions in real-time and space. Initially, photo-DSC was used for such investigations; however, this technique suffers from serious drawbacks such as a long response time of

the calorimeter and a low thermal conductivity of most of the samples, which greatly limits time resolution of the instrument. Spectroscopic techniques rely solely on chemical changes within the resin and do not provide specific information about the development of mechanical properties. Real-time FTIR spectroscopy has been combined with a rheometer to monitor both conversion and changes in rheological properties of a sample; however, this approach does not account for local spatial variations since a rheometer averages mechanical properties over the entire sample volume.

In order to address the issue of spatial variations, a quantitative approach that is suitable for in-situ monitoring of the photopolymer curing process must be developed. Ideally the technique should be able to quantify both spatial and temporal variations of mechanical properties. An approach with the ability to perform real-time investigations of the effects of parameters such as UV intensity, inhibitor concentrations, and initiator concentrations on the photopolymerization process would ultimately lead to a better understand of photopolymerization. The design and testing of such a method is the objective of this project.

1.4. Research Approach

Rheological properties of a sample play a key role in mass transport and are closely related to the microscopic structure of the sample; therefore, rheology can be used to measure structural changes during the progress of photopolymerization. In this work particle tracking microrheology is used as a tool because of its ability to accurately track changes in sample rheology as a function of both time and location. Statistical analysis of the Brownian motion of tracer particles can be used to extract rheological information

about the embedding medium as a function of time and space. This data can then be used to relate UV exposure to the polymerization and gelation of monomeric resins.

In order to test the developed methods, the microrheology of a series of photopolymerization systems (various acrylates combined with a single photoinitiator) was investigated. Previous research and the initial extracted rheological information were used to develop a standard definition of gel point for the designed method. One of the photopolymerization systems was then chosen to investigate the ability of this microrheological approach to determine the effects of several key kinetic parameters on photo-induced polymerization.

1.5. Thesis Outline

In the subsequent work, the monitoring of photo-induced free-radical polymerizations by microrheology will be discussed in detail. Chapter 2 provides a comprehensive background of photopolymerization. In Chapter 3, the concept and theory of microrheology will be reviewed and compared to other techniques that are currently used to study photopolymerization. The materials as well as the experimental and analytical procedures used in this research will be discussed in Chapter 4. The experimental results will be presented in Chapter 5, along with a comprehensive discussion. In addition to concluding remarks, the last chapter contains recommended future research and suggested uses for the experimental data obtained through this research.

CHAPTER 2

PHOTOPOLYMERIZATION

In this chapter, the process of photopolymerization will be briefly introduced and the reasons for choosing the specific systems used in this research will be explained. A more detailed discussion will be offered on general photoresins and photoinitiatiors with specific attention paid to the materials used in this study. Finally, the kinetics of the chosen system and several important applications will be examined.

2.1 Photopolymerization Overview

Photopolymerization is defined as the reaction of monomers or macromers to produce solid polymeric structures by light-induced initiation and polymerization[5]. Photopolymerization systems usually contain three main components: monomer, initiator, and additives used to impart desired properties. The chain reaction process is initiated by propagating active centers, either free radicals or cations, which are produced when light is absorbed by the photoinitiator. Linear polymer chains are obtained by reacting monomer species that contain a single double bond, while a cross-linked network of polymer chains can be formed using multifunctional monomers. The resulting solid polymer has many uses due to insolubility in organic solvents and resistance to heat and mechanical treatments[3].

Light-induced polymerization reactions offer certain advantages when compared to thermal[26] and redox polymerizations in which heat is used to produce active centers. Photopolymerization uniquely offers both spatial and temporal control of the initiation reaction through illumination control, and the production rate of active centers is often independent of temperature[6]. In addition, because active centers can be produced rapidly and efficiently using photochemical processes, photocuring offers high production rates and is more energy efficient than thermal polymerizations, which require that the entire system be heated to elevated temperatures. Photocuring systems are generally compact and solvent-free; therefore, emissions of volatile organic compounds are eliminated and material cost is reduced[2, 6].

Free-radical polymerizations account for the vast majority of photopolymerization reactions used in the industry[5]. Free-radical active centers are highly reactive and possess an unpaired electron that attacks the electron-deficient carbon double bonds, such as those found in acrylate and maleate monomers, to produce polymer chains[1]. The advantages of free-radical polymerizations are the availability of large sources of raw materials, extremely fast cure rates, well-known chemical reactions, and excellent physical properties. Free-radical polymerizations, however, have several drawbacks such as the volatility, unpleasant odor, and toxicity associated with the monomeric raw materials. In addition, free-radical polymerizations are greatly inhibited by oxygen and exhibit a high percentage of shrinkage[5, 6].

The disadvantages of free-radical polymerizations have lead to the increased study of cationic photopolymerizations. Cationic active centers attack materials containing electron-rich centers, such as the double bonds in vinyl ethers and the oxirane

groups in epoxy resins[1]. Cationic systems have two distinct advantages over free-radical systems: reduced shrinkage and the lack of oxygen inhibition. Additional benefits of cationic systems include the use of materials that have low toxicity and volatility and the continuation of polymerization after irradiation has ceased due to presence of non-terminating active centers[4]. Photoinduced cationic polymerizations, however, have the disadvantage of slower cure rates, chemical reactions that are not well understood, and the ability of water vapor to impede curing[5, 6].

The majority of research efforts devoted to photocuring have been focused on free-radical systems. Specifically, most research has been in the development and design of high performance formulations that offer rapid curing and outstanding physical and chemical end properties. This work will focus on commercially used acrylate and methacrylate free-radical systems. Special emphasis will be placed on the effect of UV penetration depth, initiator concentration, inhibitor concentration, composition of the monomer, and light intensity on the curing process.

2.2 Free-Radical Photoresins

Unsaturated monomers containing a carbon-carbon double bond are extensively used in photoinduced free-radical polymerizations. The free-radical active center reacts with the unsaturated monomer by opening the carbon double bond and adding the molecule to the growing polymer chain. The three main free-radical photopolymerization systems used are and (meth-)acrylate, thiol-ene, and unsaturated polyester systems.

2.2.1 Acrylate and Methacrylate Systems

Acrylate and methacrylate monomers are by far the most widely used in free-radical photopolymerization processes[5]. The successful commercial use of these UV-curable resins can be attributed to their high reactivity and ability to form a large variety of cross-linked polymers with taylor made properties such as color, flexibility and surface characteristics. The generalized structure of these monomers and their corresponding polymer is shown in Figure 2.1.

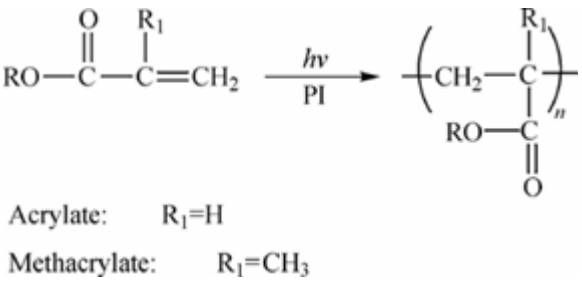

Figure 2.1: Molecular structure of a generalized acrylate monomer and its corresponding polymer repeat unit; the R side group may vary.

Studies have shown that acrylates have faster reaction rates then their methacrylate counterparts[27]. The functionality of acrylate monomers plays a key role in rheological properties and curing speed, with higher functional monomers having a higher viscosity and faster cure speed[4]. Linear acrylates are generally used as reactive diluents to reduce the viscosity of the unpolymerized liquid for ease of processing. Multifunctional acrylates increase the mechanical strength and solvent resistance of the polymer product by forming cross-linked networks rather than linear polymer chains[5, 6].

Acrylate and methacrylate systems have several drawbacks, including relatively large polymerization shrinkage and high toxicity of some monomers. Methacrylates are

considered less toxic and volatile than their acrylate counterparts[2]. Shrinkage causes stress in the polymer parts, which ultimately affects performance; it is a result of the formation of covalent bonds between monomer molecules. Covalent bonds decrease the distance between monomer molecules by approximately half compared to two molecules experiencing van der Waal's forces. Shrinkage results in a 5-25% loss in volume (2-8% in linear dimensions)[2, 6]. Thus, shrinkage places a financial burden on industries that rely on acrylate and methacrylate photopolymerization systems. The effects of shrinkage can be minimized by using oligomeric acrylates, which contain 1 to12 repeat units formed via step-growth polymerization[2, 3, 5, 6].

2.2.2 Thiol-Ene Systems

Systems that combine thiols with ene co-monomers, such as allyl ethers or acrylates were originally developed in the 1970's, but were later abandoned for acrylate systems because of unpleasant odor[6]. Renewed interest in thiol-ene systems resulted from the fact that the thiol functions as a photoinitiator by producing a thiyl and a hydrogen radical pair through a sulfur-hydrogen bond cleavage when exposed to light. Thiol-ene systems, therefore, require little or no photoinitiator in order to polymerize[4-6, 27]. As a result formulation costs are greatly reduced since photoinitiator is generally the most expensive component[27]. In addition, thiol-ene systems are also less sensitive to inhibition of oxygen and undergo less volume shrinkage compared to acrylate systems[6]. The greatest disadvantage of thiol-ene systems is the relatively slow cure rates when compared to conventional acrylate systems[5, 6].

2.2.3 Unsaturated Polyesters

Resins consisting of unsaturated polyester dissolved in styrene were among the first to be used in large scale photoinduced free-radical polymerization applications[5]. Upon illumination, the carbon double bond in the unsaturated polyester and styrene copolymerize to form a cross-linked network[1]. Figure 2.2 shows a generalized reaction scheme for an unsaturated polyester system.

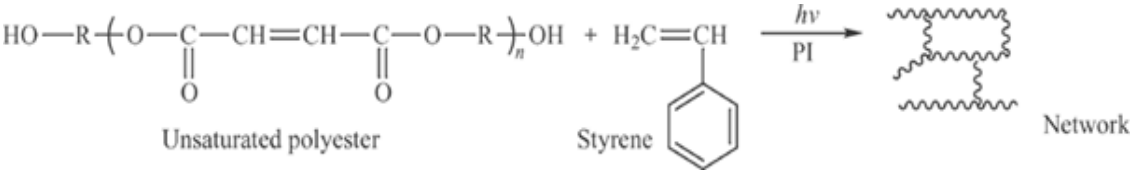

Figure 2.2: Generalized reaction scheme for an unsaturated polyester system.

The relatively slow cure, together with high volatility and the small number of monomers available, has inhibited widespread use and further development of the system. Unsaturated polyesters are mainly used in the low-tech wood finishing industry because of relatively low material cost[5, 6].

2.3 Photoinitiators

Since most of the commonly used monomers do not produce free-radicals when exposed to UV light, it is necessary to include photoinitiators to initiate the polymerization process by producing free-radicals upon illumination. Upon absorption of light with a specific frequency, the photoinitiator molecule is promoted from the ground electronic state to either a singlet or triplet excited electronic state. These excited molecules then undergo cleavage or react with another molecule to produce initiating free

radicals[1]. The photoinitiator plays a key role in that it governs both the rate of initiation and the penetration of the incident light into the sample as a result of absorption, and therefore cure depth[5]. Only free-radical photoinitiator systems, commonly classified as type I and type II, will be described here.

2.3.1 Unimolecular Photoinitiators (Type I)

Type I photoinitiators are usually termed unimolecular because the initiation system involves only one molecular species interacting with the light and producing free-radicals. One class involves photoinitiators that form radicals through cleavage of the initiator molecule as shown in Figure 2.3[5]. This cleavage may take place at the α or β position with respect to the carbonyl group. Cleavage occurs mainly in aromatic carbonyl compounds; α-cleavage occurs if the bond adjacent to the carbonyl is broken to produce two free radicals, one benzoyl and one fragment radical[1, 6]. The benzoyl radical is the major initiating species, while the fragment in some cases may or may not contribute to the initiation[6]. β-cleavage occurs predominately in photoinitiators with a carbon-sulfur bond or a carbon-oxygen bond adjacent to the benzoyl chromophore[1, 6]. A second class of unimolecular photoinitiator includes those that form biradicals through intramolecular hydrogen abstraction as shown in Figure 2.4[6]. This mechanism commonly occurs in ketones and results in a ketyl radical, which participates in termination, and another radical that induces growth of the polymer chain.

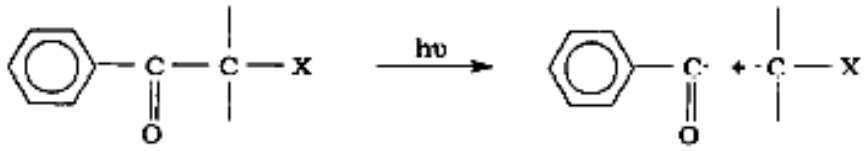

Figure 2.3: Cleavage mechanism of unimolecular photoinitiator free-radical generation[5].

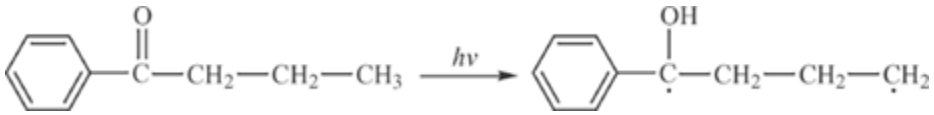

Figure 2.4: Hydrogen abstraction mechanism of unimolecular photoinitiator free-radical generation between the photoinitiator benzophenone and the hydrogen donor tetrahydrofuran[6].

2.3.2 Bimolecular Photoinitiator Systems (Type II)

If the photoinitiator in its excited state interacts with a second co-initiating molecule to generate radicals by a bimolecular reaction as shown in Figure 2.5[6], the initiating system is termed bimolecular or Type II. Once the photoinitiator is in the excited state, the co-initiator, which is usually an ether or an alcohol, serves as a hydrogen or electron donor. The reaction results in the formation of free-radicals, one or more of which may actually begin the photopolymerization process. Photoinitiator families of this class include benzophenone derivatives, thioxanthones, camphorquinones, benzyls, and ketocoumarins[5, 6].

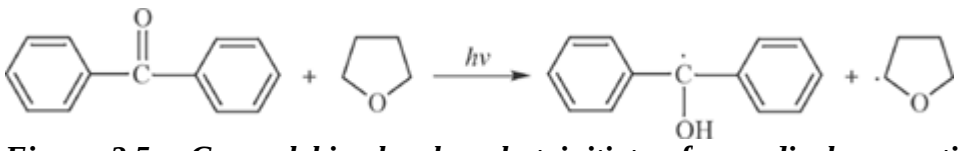

Figure 2.5: General bimolecular photoinitiator free-radical generation mechanism shown for intramolecular H-abstraction of photoinitiator 1-phyenyl-butan-1-one[6].

Bimolecular systems require longer wavelengths and, therefore, less energy than unimolecular systems, which are typically constrained to use in the UV region of the spectrum because of the absorption characteristics of the benzoyl chromophore. The production of free-radicals in bimolecular systems, however, decreases in vitrifying systems because diffusion of the initiator and co-initiator molecules is strongly suppressed[1, 6].

2.3.3 Photosensitizers

In the bimolecular systems described above, the co-initiator will not absorb light to initiate polymerization. In contrast, photosensitizers that are able to absorb light are often used to enhance the photopolymerization. Photosensitizers are used to extend the optical window of the system when a monomer or pigment absorbs in the same region as the photoinitiator[1, 6]. They are used to improve initiation efficiency by absorbing photons from the light source that the photoinitiator absorbs with low efficiency, or not at all[5]. Two mechanisms have been identified to describe the interaction between photosensitizers and photoinitiators: energy transfer and electron transfer. In energy transfer the photosensitizer absorbs the light and transfers the energy to the photoinitiator in order to produce initiating free radicals. In the more common electron transfer mechanism the photosensitizer becomes excited when illuminated and forms an excimer with the photoinitiator, which then allows electron transfer from the photoinitiator to the photosensitizer, thereby producing two radicals[1].

2.4 Kinetics

A description of free-radical kinetics must take into account three basic steps: initiation, which creates free-radical active centers; propagation, which grows the polymer chains; and termination, which destroys the active centers and ends chain growth. The kinetics of linear and multifunctional monomer systems vary only in the way the chain is propagated and free-radicals are terminated. Figure 2.6[5] outlines the basic steps of free-radical photopolymerization of a linear photoresin. The kinetics of a multifunctional photoresin are more complicated and include cross-linking as shown in Figure 2.7[5]. Another important aspect of free-radical kinetics is the inhibition of the process. Discussion of photopolymerization kinetics will be limited to free-radical photopolymerizations since the kinetics of cationic photopolymerization are not well understood.

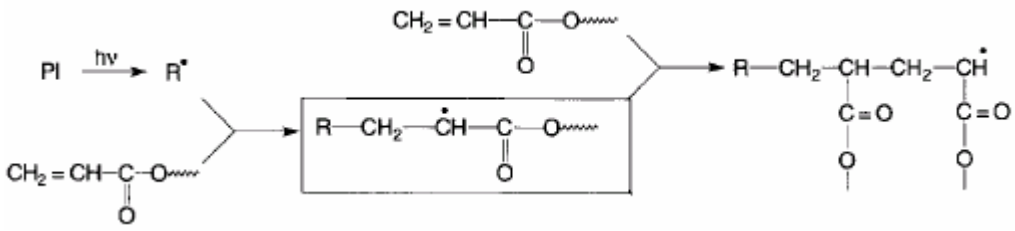

Figure 2.6: Schematic representation of linear photopolymerization kinetics[5].

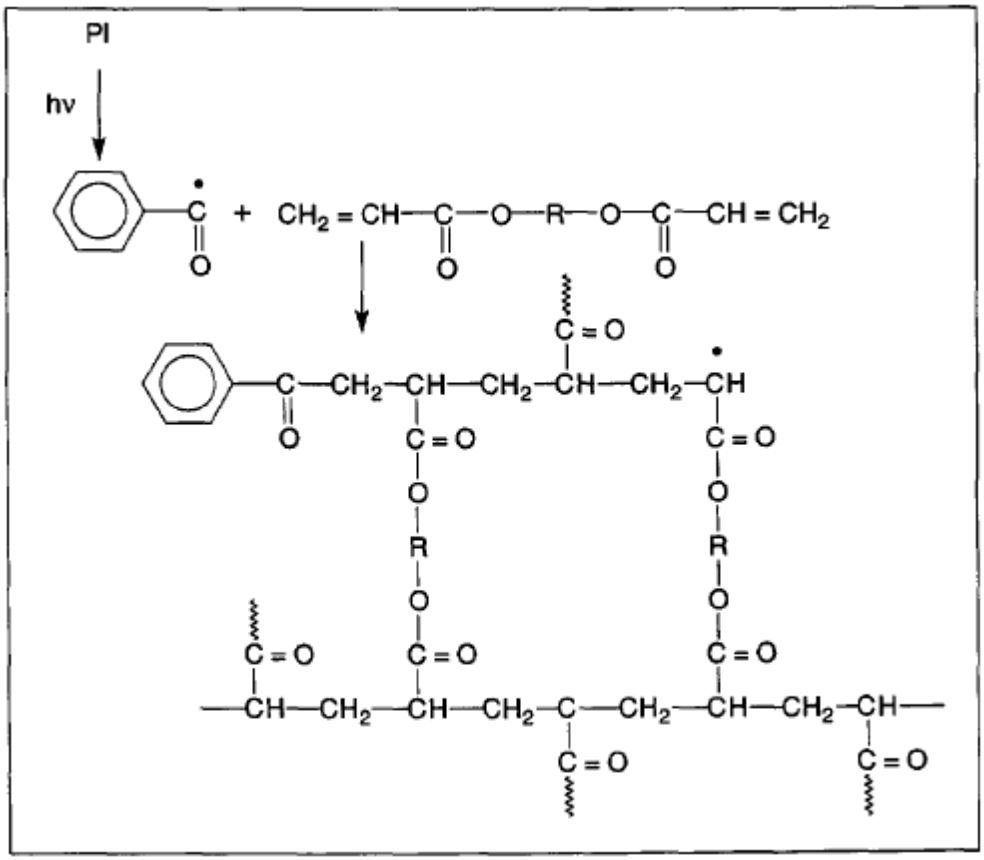

Figure 2.7: Schematic representation of the kinetics of a multifunctional photopolymerization reaction[5].

2.4.1 Initiation

In photoinduced free-radical polymerization, the rate of initiation depends on two processes: the dissociation of the initiator and the initiation of the propagating chain. The basic equations for initiation are:

$$In \xrightarrow{h\nu} R^{\bullet} \tag{2.1}$$

$$R^{\bullet} + M \xrightarrow{k_i} M_n^{\bullet} \tag{2.2}$$

where *In* is the photoinitiator and $R^{\bullet}$ is a free-radical. The main mechanisms of radical generation are by photocleavage of aromatic carbonyl compounds, which undergo a Norrish type 1 bond scission and by hydrogen abstraction from a hydrogen donating molecule, to generate a ketyl radical and a donor radical (see section 2.3)[1, 5].

The rate at which photons are absorbed at a specific wavelength will determine the decomposition rate of photoinitiators, and ultimately the initiation of the propagating chain[5]. An important parameter in the rate of initiation is the amount of photons absorbed by the photoinitiator molecules, I_a, which is commonly expressed in (mol photon/L•s). Beer's Law, which relates the absorption of light to the concentration of the absorbing species, is used to define I_a for a specified wavelength of light. Beer's Law originates from the partial differential equation used to describe the intensity of light passing through an absorbing medium:

$$\frac{dI}{dx} = -kI \tag{2.3}$$

where I is the intensity and k is the absorption coefficient. The absorption coefficient combines the terms of molar absorptivity, ε, (in cm^{-1} M^{-1}) and concentration of absorbing species [I] (in M) into a single term with the units of inverse centimeters[1, 6]. Equation 2.3 can be integrated to ultimately yield:

$$I_a = I_0 \exp(-kx) \tag{2.4}$$

where I_0 is the intensity of the incident light[1, 6]. Essentially, Beer's Law states that there is an exponential dependence between the transmission of light through an absorbing medium and the absorption coefficient, k, which is often a linear function of the concentration of the absorbing species. Analysis of Beer's Law with respect to

photopolymerization has shown that the optimum value of I_a depends on the concentration of photoinitiator[1]. For example, in a thick sample simply increasing the amount of photoinitiator does not result in a homogeneous reaction rate since upper layers of the sample will absorb the largest fraction of incident light, limiting initiation near the bottom of the sample.

2.4.2 Propagation

Free-radical photoinitiated polymerization usually follows chain growth polymerization kinetics; therefore, propagation involves the addition of monomer to the growing polymer chain as shown in the following basic equation:

$$M_n^{\bullet} + M \xrightarrow{k_p} M_{n+1}^{\bullet} \tag{2.5}$$

where M is the monomeric photoresin and $M_n^{\bullet}$ represents a growing polymer chain. The propagation step is where physical and chemical changes in the photopolymerization system begin to become more evident. The rate of propagation is primarily dependent on the functionality of the monomer[5]. For linear monomers the propagation step is marked by a steady increase in both viscosity and elastic modulus resulting from spatial hindrance associated with continued chain elongation. Multifunctional monomers undergo a more rapid change in both viscosity and elastic modulus due to the formation of dense cross-linked networks, which ultimately leads to the creation of a solid polymer. Increasing the monomer functionality accelerates the curing reaction, but also reduces the final degree of conversion, because gelation of the irradiated sample restricts the mobility of the reactive species and prevents completion of the polymerization reaction[1].

2.4.3 Termination

Termination of free-radical active centers may occur either by combination or by disproportionation[1, 5, 6]. In termination by combination, two propagating chains unite to form one long polymer molecule:

$$M_n^{\bullet} + M_m^{\bullet} \xrightarrow{k_{tc}} M_{n+m} \tag{2.6}$$

In termination by disproportionation, one propagating chain abstracts a hydrogen atom from a neighboring propagating chain, resulting in two polymer molecules, one of them having a terminal double bond:

$$M_n^{\bullet} + M_m^{\bullet} \xrightarrow{k_{td}} M_n + M_m \tag{2.7}$$

The rate of termination for linear monomers, which is generally assumed to be independent of chain length, equals the rate of destruction of propagating active centers[1]. Termination mechanisms are more complex for multifunctional monomers because free-radical center trapping and effects of reaction—diffusion must be considered[5]. As a result of cross-linking in multifunctional monomers, free-radicals often become trapped in the network and are unable to react further. This often leaves a substantial amount of unterminated active centers and unreacted double bonds in cross-linked polymer systems[1].

2.4.4 Inhibition

One of the major disadvantages of free-radical photopolymerization is its susceptibility to oxygen inhibition. This inhibition is particularly problematic in thin-film and coating applications where oxygen diffusion plays a significant role in increasing cure times, which often results in incomplete conversion at exposed surfaces[28, 29]. When

oxygen, which is essentially a biradical in its electronic ground state, reacts with a free-radical, it forms a peroxy radical, which is much less reactive[1]:

$$M^{\bullet} + O_2 \xrightarrow{k_o} M - O - O^{\bullet} \quad (2.8)$$

$$M - O - O^{\bullet} + M \longrightarrow No \quad Rxn \quad (2.9)$$

Hence, oxygen effectively acts as a chain terminator and reduces the rate of polymerization until all oxygen in the system has been consumed[1].

Costs associated with combating the effects of oxygen inhibition are high. One way to minimize the effect is to blanket the system with an inert gas such as nitrogen, carbon dioxide, or argon[28, 29]. Waxes or shielding films may also be used to prevent oxygen from entering the system. Other methods include adding oxygen scavengers, dye sensitizers, or antioxidants to capture oxygen and prevent it from reacting with propagating chains[1]. High concentrations of photoinitiator or increased light intensity may also be used to increase the production of free-radicals in order to consume the oxygen within the system more rapidly. The last method, however, is ineffective close to the surface because it becomes difficult to consume the oxygen faster than it diffuses into the sample[28, 29].

Formulators knowingly introduce polymerization inhibitors, such as hydroquinone (HQ) and hydroquinone monomethyl ether (MEHQ), in order to promote process and shelf stability of highly reactive acrylate monomer based formulations. The inhibitors act by reacting with the initiating and propagating free-radicals and converting them either to nonradical species or low reactive radicals that are unable to promote propagation:

$$M^{\bullet} + Z \xrightarrow{k_z} M + Z^{\bullet} \quad (2.10)$$

$$M^{\bullet} + Z \xrightarrow{k_z} MZ^{\bullet} \quad (2.11)$$

$$M + Z^{\bullet} or\ MZ^{\bullet} + M \longrightarrow No\ Rxn \quad (2.13)$$

When used in small amounts, inhibitors can scavenge free-radicals that form during the manufacturing process or storage, without negatively effecting cure time or final properties. The concentration of inhibitor is dependent on the inherent instability and functionality of the monomer. Once all the inhibitor is consumed, the polymerization will proceed as usual.

2.4.5 Summary of Basic Kinetic Equations

The general kinetic reactions of photo-induced free-radical polymerization can be summarized by the following list of equations:

Initiation:

$$I \xrightarrow{h\nu} R^{\bullet} \quad (2.13)$$

$$R^{\bullet} + M_n \xrightarrow{k_i} M_n^{\bullet} \quad (2.14)$$

Propagation:

$$M_n^{\bullet} + M \xrightarrow{k_p} M_{n+1}{}^{\bullet} \quad (2.15)$$

Termination:

$$M_n^{\bullet} + M_m^{\bullet} \xrightarrow{k_{tc}} M_{n+m} \quad (2.16)$$

$$M_n^{\bullet} + M_m^{\bullet} \xrightarrow{k_{td}} M_n + M_m \quad (2.17)$$

Inhibition by Oxygen:

$$M^{\bullet} + O_2 \longrightarrow M - O - O^{\bullet} \quad (2.18)$$

$$M - O - O^{\bullet} + M \longrightarrow No \;\; Rxn \quad (2.19)$$

Polymerization Inhibitors:

$$M^{\bullet} + Z \xrightarrow{k_z} M + Z^{\bullet} \quad (2.20)$$

$$M^{\bullet} + Z \xrightarrow{k_z} MZ^{\bullet} \quad (2.21)$$

$$M + Z^{\bullet} or\, MZ^{\bullet} + M \longrightarrow No\;\; Rxn \quad (2.22)$$

This list of equations will be referred to in the results and discussion chapter of this work. Specifically, Equations 2.13-2.22 will be used to illustrate the effects of varying experimental parameters on certain elements of this kinetic network.

2.5 Gelation Theory

The liquid-to-solid transition during the polymerization of monomeric materials is marked by a point of gelation, which in free-radical photopolymerization is the result of chain elongation and the formation of densely cross-linked networks. The transition is often preceded by a rapid increase in viscosity; therefore, gelation can readily be detected with rheological techniques. There are two different types of gelation: chemical gelation, which result from the formation of chemical bonds and physical gelation, which result from the growth of physically connected aggregates. The principal distinction between chemical and physical gelation is the lifetime of the junctions. Chemical bonds are considered permanent while physical junctions due to intermolecular association are finite, constantly being formed and destroyed at such slow rates that the network appears to be permanently connected.

The development of equilibrium mechanical properties during gelation is graphically illustrated in Figure 2.8[30]. As connectivity builds, the steady shear viscosity of the liquid, η, sample grows quickly in the approach to gelation and diverges to infinity at the point of gelation. At the gel point, the equilibrium modulus, G_∞, remains near zero because the stress in a deformed gel can still relax completely; however, beyond the point of gelation the equilibrium modulus starts to increasingly develop. The rheological behavior at the point of gelation is unique in that infinite time is required for stress relaxation, which in a broad distribution of shorter self-similar modes.

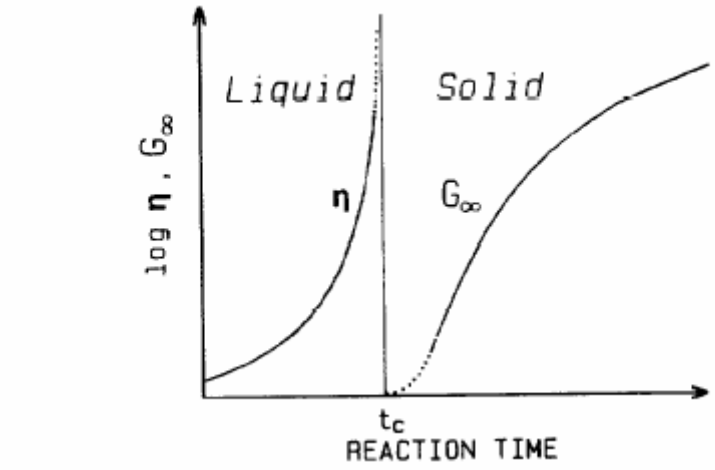

Figure 2.8: Steady shear viscosity and equilibrium modulus of a crossing-linking polymer as a function of reaction time.[30]

The photoresin remains a liquid polymer until a critical degree of conversion is reached, which is theoretically equivalent to the gel point[31, 32]. Classical mean-field theories with the ability to predict the critical conversion with reasonable accuracy have been developed[31]. The predictive theories are based on the assumptions that all functional groups of the same type are equally reactive, all groups react independently of one another, and intramolecular condensation does not occur. Flory developed a

parameter, α, which can be used to predict the threshold conversion. The Flory parameter depends on the geometry of the network-forming species and is defined as the probability that a given functional group of a branch unit leads, via a chain of bifunctional units, to another branch unit. For homopolymerization, the Flory parameter is defined as[32]:

$$\alpha_c = \frac{1}{1-f} \tag{2.23}$$

where *f* is the functionality of the branching unit, which is defined by Flory as the number of other molecules that can react with the network-forming species. For example a trifunctional monomer has the ability to bond with six other molecules; therefore, according to Flory the monomer would have a functionality *f*=6. The bifunctional acrylate in Figure 2.7 can connect with four molecules, and thus *f*=4. Monomers with higher functionality form infinite cross-linked networks more rapidly than ones with lower functionality. As a result, monomers with higher functionality have to reach a lower critical degree of conversion for gelation to occur. After reaching this threshold conversion, lower functional monomers proceed to higher final conversions as a result of less steric hindrance.

Measurements to determine the instant of gelation can be obtained using several techniques, including rheology and light scattering. Equilibrium rheological techniques, which subject the sample to shear flow, are able to estimate the position of the gel point by extrapolating the appearance of an equilibrium modulus or the divergence of the steady shear viscosity (see Figure 2.8). The major shortcoming of such equilibrium measurements is that the apparent gel point, not the real gel point, is yielded as a result of extrapolation of an experiment that can never really reach equilibrium[33]. Transient

rheological techniques, such as dynamic mechanical analysis, apply small amplitude oscillatory shear to the sample. These techniques are better suited for determining the gel point because no extrapolation is required and the instant of gelation can be measured as accurately as the rheometer permits. Dynamic light scattering allows for the nondestructive, real-time determination of both the gel point and the critical dynamics near the point of gelation[33]. Techniques such as spectroscopy and calorimetry are used to measure the critical degree of conversion at the gel point.

There are several definitions and classifications of gelation in current rheological research; however, nearly all definitions are based on the Winter-Chambon criteria first developed in 1986[30]. Winter and Chambon used transient rheological techniques to investigate the chemical gelation of polydimethylsiloxane (PDMS). The researchers determined that at the gel point, loss and storage moduli, G'' and G', were congruent and proportional to $\omega^{0.5}$ over several decades of frequency and a wide range of temperatures[30, 33]. The independence of the loss tangent on the frequency of the dynamic experiment was found to be another characteristic of the gel point. Winter and Chambon introduced a general constitutive equation for critical gels that is predictive for all known rheological properties, based on the single material parameter of gel strength[30].

2.6 Applications

Traditionally, free-radical polymerization has been applied to thin films and coatings where light penetration is generally less of an issue, high production speeds can be achieved, and formulations free from volatile emissions are desirable[2-4]. This type of application allows for the minimization of the disadvantages of free-radical

photopolymerization such as shrinkage and poor conversion in thick or strongly absorbing systems. Despite the limitations of free-radical photopolymerization, applications are far-reaching, encompassing the automotive, electronic, medical, optical, graphical arts, flooring, and furniture industries. Research in photopolymerization continues to fuel the expansion of this list to include areas of rapid prototyping and biomedical implants. A few relevant applications are highlighted below.

2.6.1 Films, Coatings, and Adhesives

Photopolymers may be used as coatings for a wide range of substrates, including wood, glass, paper, metals, and plastics. These coatings serve to protect surfaces from scratches and chemical exposure, to provide decoration and color, and to allow modification of surface properties[3, 27]. Currently, most coatings are applied as a liquid monomer formulation and then photopolymerized; however, photocurable powder coatings are being developed and are expected to have a huge impact on the metal, paper, and wood coating industries[2]. Photopolymerized adhesives provide bonding between laminates, such as glass panes or plastic films. In addition, adhesives and release coatings are used to make tapes, labels, and stickers[2, 4]. Photocurable inks are used on packaging materials and magazines[2].

2.6.2 Biomaterials

Photopolymerization has become more prominent in biological applications in recent years because it offers rapid reaction rates and superior products. Photopolymerization for biological applications, however, is often more challenging

because reactions usually have to occur under visible light and the end product must have zero toxicity[6]. Scaffolding for bone and tissue engineering, bioadhesives for wound closure, and microchips for biochemical analysis are examples of biomaterials produced using free-radical photopolymerizations. Cross-linked hydrophilic polymer networks that are used in applications like contact lenses and drug delivery are also produced using free-radical photopolymerization[34].

2.6.3 Stereolithography

Stereolithography is a rapid prototyping technique that translates CAD files into three-dimensional solid objects one layer at a time by tracing a laser beam or ultraviolet light on the surface of a vat of liquid photopolymer. The resin solidifies wherever it is exposed to light, resulting in a solid layer. The process is repeated, layer-by-layer, until the 3-D object is completely built. Figure 2.9[35] gives a schematic diagram of the process. The ability of stereolithography to produce three-dimensional solids from CAD files within a matter of hours has made it the most widely used rapid prototyping technology. Significant limitations such as the inability to increase part building speeds without loss of accuracy, part size distortions of the final product relative to the CAD design, and spatial resolution limitations that are considerably greater than inherent optical limits are hindering further advancements in the field of stereolithography.

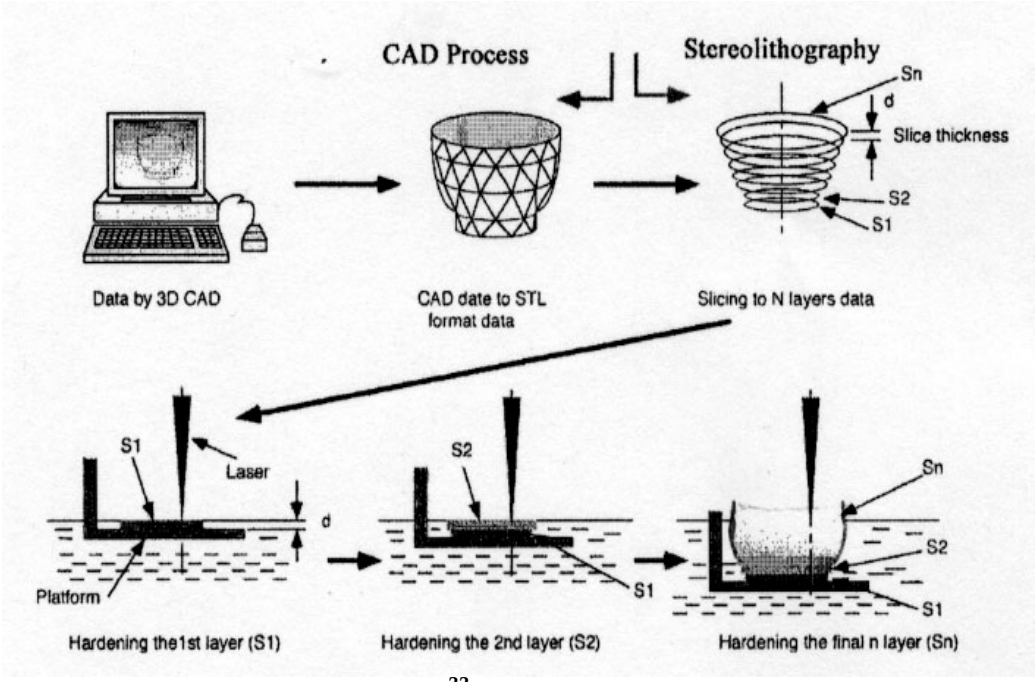

Figure 2.9: Process of stereolithography[33]

CHAPTER 3

MICRORHEOLOGY

In this chapter, the technique of microrheology will be introduced and special attention will be given to the area of passive microrheology. The method and theory behind particle tracking microrheology will be discussed. Finally, the technique will be compared in detail to other methods currently being used to study photopolymerization.

3.1 Overview of Microrheology

Rheology is the study of the deformation and flow of matter; microrheology simply expands this definition to microscopic length scales. Microrheology is predominantly used to experimentally probe the mechanical properties of soft materials. In contrast to traditional rheology methods where bulk properties are measured and the sample is subjected to an externally imposed shear strain, microrheology relies on the Brownian motion of micron-sized particles embedded in the sample to assess the viscoelastic properties of the surrounding medium. The principle advantages of this technique are that it requires only a microscopic amount of material to perform a detailed rheological study and that it can be used to probe the local properties of rheologically inhomogeneous materials. In addition, microrheology is able to probe a much larger frequency range than traditional macrorheology and because microrheology uses only thermally generated forces, it can be used to nondestructively measure even extremely

fragile materials[36]. As a result of these strengths, microrheology has lead to advancements in several research areas of complex fluids including living cells, proteins, hydrogels, colloids near the glass transition, and various soft biomaterials[37].

There are two main categories of microrheology techniques: passive, which tracks the random motion of tracer particles due to thermal fluctuations and active, where an external force, usually created with optical tweezers or magnetic fields, is applied to the probe particles in order to measure rheological properties. Passive techniques are useful for measuring low values of predominantly viscous moduli, where active techniques can be extended to measurable range of samples containing significant amounts of elasticity[36]. Active microrheology methods also allow the option of measuring stress relaxation of a complex fluid under the influence of an external force[37]. Passive particle tracking microrheology, however, is better studied, less invasive to the sample, and more cost effective compared to active microrheology techniques[36-38].

3.2 Theory of Particle Tracking Microrheology

The fundamental assumption of passive particle tracking microrheology is that the Brownian dynamics of microscopic particles embedded within a fluid is determined by the mechanical properties of the surrounding environment. Passive techniques rely solely on the thermal energy of the embedded tracer particles, k_BT, to measure rheological properties; therefore, it is essential that measurements be performed on materials that are sufficiently soft in order for the thermal motion of the tracer particles to be detectable. A typical experimental setup employs video-microscopy to track the Brownian motion of micron-sized, inert, fluorescent particles[39]. Information about the local mechanical

properties of the sample is then obtained by performing statistical analysis of the tracer particle motion. Figure 3.1 illustrates the principle steps, many of which are explained in detail below, of particle tracking microrheology.

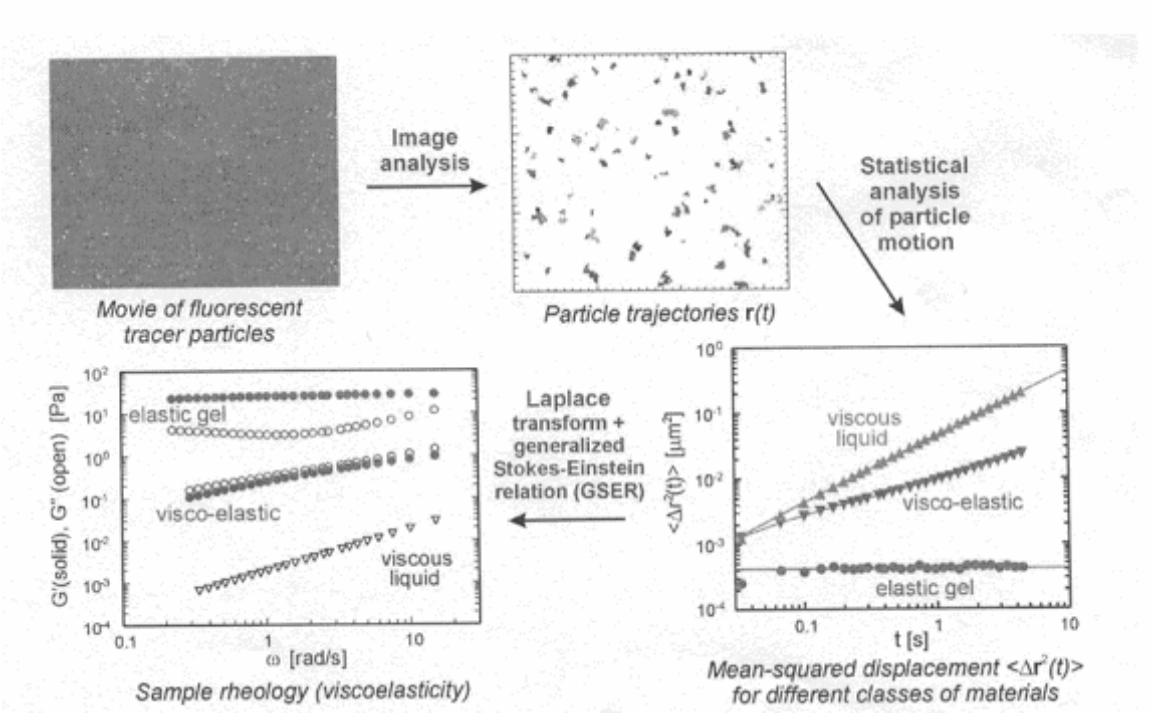

Figure 3.1: Principles of particle tracking microrheology: from particle motion to sample rheology.

The motion of the particles in a Newtonian liquid is diffusive and the diffusion coefficient is given by the Stokes-Einstein relation $D = k_bT/6\pi\eta a$. For diffusive motion, the mean-squared displacement is defined as[38]:

$$\left\langle \Delta r^2(\tau) \right\rangle \equiv \left\langle \left| r(t+\tau) - r(t) \right|^2 \right\rangle = 2\,d\,D\,\tau = \frac{d\,k_b\,T}{3\,\pi\,\eta\,a}\,\tau \qquad (3.1)$$

where Δr is the MSD, k_B is Boltzmann's constant, T is the absolute temperature, d is the dimensionality of the system, a is the particle radius, the brackets designate averaging over all starting times t and τ is the lag time. The Stokes-Einstein relation enables

viscosity measurements by monitoring the time-dependent MSD of a particle of known size.

Particles implanted in a completely elastic environment will have a maximum displacement that occurs when the thermal energy is equal to the elastic energy of the deformed cross-linked network[38]. As a result, MSD approaches a plateau for long lag times:

$$\left\langle \Delta r^2 \right\rangle_{\tau\to\infty} = \frac{d\,k_b T}{3\pi G a} \tag{3.2}$$

where G is the storage modulus of the elastic medium[38].

Complex fluids, materials that are neither Newtonian liquid or completely elastic, exhibit much more complex behaviors including a frequency dependent complex viscoelastic response modulus with both viscous and elastic components: $G^*(\omega) = G'(\omega) + iG''(\omega)$[38]. The fundamental basis of particle tracking microrheology in complex fluids is the application of the generalized Stokes-Einstein relation (GSER) for a sphere in a homogeneous, incompressible fluid, which takes the form (after a Laplace transform)[36-38]:

$$\left\langle \Delta \tilde{r}^2(s) \right\rangle = \frac{d\,k_b T}{3\pi a\, s\, \tilde{G}(s)} \tag{3.3}$$

where s is the Laplace frequency, $\Delta \tilde{r}^2(s)$ is the MSD of the particle, and $\tilde{G}(s)$ is a frequency-dependent modulus (the single real function). The GSER is essential to particle tracking microrheology because it translates the microrheological measurement of MSD into the macroscopic measurements of viscosity or elasticity. Both the viscous and elastic response can be determined by calculating the complex viscoelastic modulus from $\tilde{G}(s)$, which is possible since the real and imaginary part are related to each other

through the Kramers-Kronig relations[38]. The frequency range where Equation 3.3 remains valid is dependent on both the inertia and compressibility of the system, but includes the typical range of videomicroscopy, 0.1-60 Hz[38].

3.3 Techniques Used to Study Photopolymerization

Several techniques are currently used to study photo-induced polymerization. Techniques such as infrared spectroscopy and calorimetry rely on reaction kinetics, while techniques like rheometry rely on changes in mechanical properties to monitor the progress of photopolymerization. In this section the most commonly used techniques will be described and compared to particle tracking microrheology.

3.3.1 Spectroscopy

Spectroscopy is the branch of physics concerned with the production, measurement, and interpretation of electromagnetic spectra arising from either emission or absorption of radiant energy by various substances[40]. Two methods of studying photopolymerization using spectroscopy have been well established: infrared and Raman spectroscopy[10, 11, 40-42]. Infrared (IR) and Raman spectroscopy both measure the vibrational energies of molecules and can be used to obtain both conversion and rate of polymerization the two methods rely on different selection rules for spectral information[40, 42]. Peaks in the spectra correlate to functional groups within a molecule. As monomer is converted to polymer, the height of peaks associated with the monomer specific bonds decreases. The conversion may then be calculated as the ratio of this peak height (or area) at any point in time to the initial peak height (or area). The rate of

polymerization is calculated by differentiating the conversion curve with respect to time[41].

Fourier transform infrared (FTIR) is one of the most commonly used IR analysis methods for determining the composition of polymers. FTIR measures the vibrational energies of atoms or specific groups of atoms within a molecule as well as rotational energies. The FTIR technique identifies components by comparing the spectrum of a sample to reference spectra[42]. FTIR spectroscopy allows rapid multiple scanning of a sample; therefore, the technique has permitted real-time observation of changes in the spectra[40]. As a result, this method is commonly used to follow the cure reaction of photo-induced polymerizations[41].

Raman spectroscopy is based on the Raman effect, which is the inelastic scattering of photons by molecules; therefore, it is an emission phenomenon as opposed to IR absorption, and results from vibrations caused by changes in polarizability[40, 42]. Raman spectroscopy is particularly useful when studying aqueous solutions, wet samples, or where differentiation between polymers with similar structures is necessary[41]. Raman spectroscopy has several advantages compared to FTIR spectroscopy, such as higher quantum efficiency, the ability to study lower frequency vibrations, and higher spatial resolution as a result of shorter excitation wavelengths[11]. The Raman technique has the disadvantages of being slower and more costly. Infrared spectroscopy and Raman spectroscopy are considered complementary techniques, because the selection rules are different[41].

3.3.2 Calorimetry

Calorimetry, which measures heat flow into a material (endothermic) or out of a material (exothermic), is categorized into adiabatic calorimetry, covering the temperature range from 10 to 400 K, and differential scanning calorimetry (DSC), covering the temperature range from 200 to 1000 K[43]. Photodifferential scanning calorimetry (PDSC) is a standard technique for obtaining the rate of polymerization and conversion[41, 43]. The conversion of monomer carbon double bonds to polymer carbon single bonds is an exothermic reaction. The heat flow from the sample (ΔH in W/g) is directly proportional to the rate of polymerization[41]:

$$R_p = \frac{\rho \Delta H}{\Delta H_p} \tag{3.4}$$

where R_p is the rate of polymerization, ρ is the density of the monomer (g/L) and ΔH_p is the heat of polymerization for the reactive group of the monomer (J/mol). The conversion of the sample is calculated by integrating the area under the rate of polymerization versus time curve[41]. Calorimetry is advantageous because it is not affected by cross-linking reactions and offers direct measurement of the polymerization rate[7]; however, this technique suffers from serious drawbacks such as a long response time of the calorimeter and a low thermal conductivity of most samples, which greatly limits temporal resolution[8]. As a result, spectroscopy methods are preferred for performing real-time measurements.

3.3.3 Rheology

Reaction kinetics are traditionally the most common measurement used to monitor the progress of photopolymerization as a function of time; however, it is difficult

to extract spatial information about the photopolymerization process from reaction kinetics. Moreover, bond conversion rates measured with calorimetry or spectroscopy are not the most predictive indicator of product quality, which remains the primary focus of the majority of photo-induced polymerization applications. The most relevant parameter in controlling the final product is the transition in mechanical properties from a liquid monomeric resin to a highly cross-linked gel. Analysis of bond conversion rates in terms of sample rheology requires significant model assumptions, which often leads to inaccurate data and poor ability to control the system. As a result, the direct measurement of mechanical properties during gelation of a photoresin is the preferable approach.

As mentioned at the beginning of this chapter, when exposed to UV irradiation, photoresins react and increase their molecular weight as they form polymer networks. As the network builds, the viscosity increases, which can easily be detected using rheological techniques. In order to study photopolymerization with a rheometer, the sample geometry (mostly parallel plate) must be adapted to accommodate UV irradiation. The general experimental setup, first developed by Khan *et al.*[17], has the top plate holder scooped out to permit the insertion of a 45 mirror, which is used to reflect the UV light onto the sample. The sample is then squeezed between two parallel plates made from optical glass[14-18, 21, 22, 24]. During rheological measurement the sample can then be exposed to UV light. Steady shear rheological methods are good for precisely measuring the viscosity early in the curing and up to the gel point. If viscosity measurements are required over the entire conversion range, then steady shearing rheometry is not the recommended choice since continuous shear would disrupt gelation[41]. In addition, large

torques will build up after the gel point and could potentially damage the torque transducers[16].

Dynamic mechanical methods, typically oscillatory parallel plate rheometry, are commonly used to measure the dynamic mechanical properties from the liquid state to the solid state. By using small-amplitude oscillatory deformations, the dynamic storage and loss moduli can be obtained. These quantities can then be used to calculate the viscosity and gel modulus[45]. Whereas steady shear rheometry can measure the initial stages of cure up to the gel point, dynamic mechanical analysis (DMA) can measure the entire cure process all the way to the completion of cure, although the method is too insensitive to measure low-viscosity liquids. In addition, DMA can be used to measure the properties of final cured samples[45]. Both steady shear rheological methods and DMA are often combined with spectroscopy techniques in order to simultaneous obtain real-time kinetic and mechanical data[17, 18, 24].

The direct measurement of mechanical properties using traditional rheometers adapted to accommodate UV light sources has provided useful insight into photopolymerization. This technique, however, has important drawbacks such as the dimension of the sample, averaging of sample properties, and externally applied stress. Conventional rheometers require large amounts of sample, typically in the range of milliliters, which makes it near impossible to study rare or precious materials[36]. In order for accurate results to be obtained the sample must be at least 25 mm in diameter and 100-500 μm thick. Also, investigating thin samples with a standard rheometer increases the risk of plates grinding against each other when shrinkage occurs[16]. In addition, modeling results have shown that the intensity of UV irradiation can vary significantly

due to absorption in the resin by photoinitiator. In view of that, the mechanical properties, represented by G^*, will be a function of both time and location. Conventional rheometers average over the entire sample volume; therefore, detailed spatial information is entirely lost in the complex viscoelastic modulus when measured with a mechanical rheometer. Finally, mechanical rheometers apply an external stress to deform a sample. Although the deformations are considered small, they can influence the overall photopolymerization process.

To address the above issues, microrheology has emerged as a new way to study the process of photopolymerization, by monitoring the local mechanical properties of a sample. Microrheology has the distinct ability to utilize microliter amounts of material to accurately track changes in sample rheology as a function of both time and location. In addition, the experimental setup associated with microrheology is considerably more cost effective than the methods describe above since it simply requires a camera, computer and microscope[37].

CHAPTER 4

EXPERIMENTAL

In this chapter a detailed description is provided of the materials, techniques, and equipment used to perform this study of in-situ monitoring of photopolymerization using microrheology. The experimental chapter is divided into three main parts: photopolymerization system, experimental design, and analytical procedures.

4.1 Photopolymerization System

As stated in Chapter 2, the primary components of a photopolymerization system are monomeric photoresin and photoinitiator. For microrheology it is necessary to introduce fluorescent tracer particles to the system as well. Various combinations of monomer and initiator were studied.

4.1.1 Monomer

Acrylate monomers are highly reactive and well studied, which makes them an ideal system to investigate. Three commercially produced acrylate monomers were obtained from Sartomer Company (Exton, PA.) each with a different functionality: SR494, SR351, and SR272. SR494, ethoxylated pentaerythritol tetraacrylate, is a heat resistant, fast curing tetrafunctional monomer with the following chemical structure:

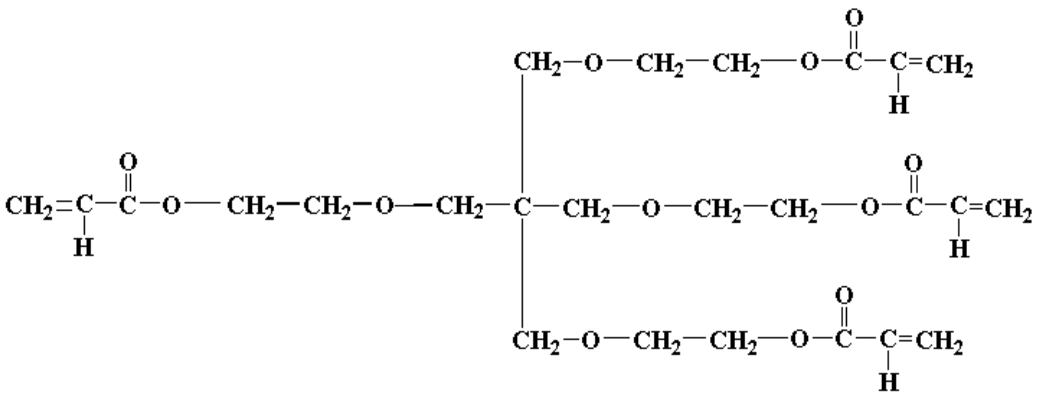

SR494 has four carbon double bonds; therefore, it is the most reactive of the monomers investigated and is able to rapidly for dense cross-linked networks. SR351, trimethylolpropane triacrylate (TMPTA), is a low viscosity, fast curing trifunctional monomer with the following chemical structure:

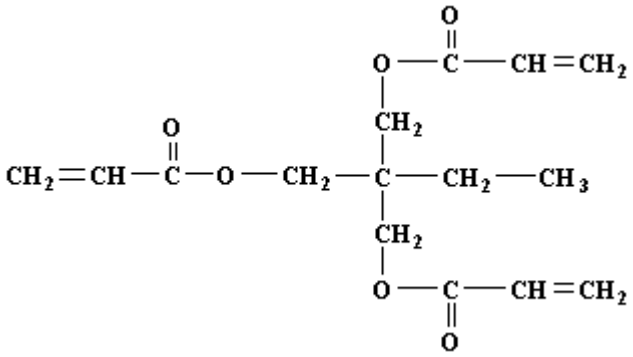

SR351 is considered less reactive than SR494 because it has only three carbon double bonds. SR272, triethylene glycol diacrylate, is the difunctional monomer shown below:

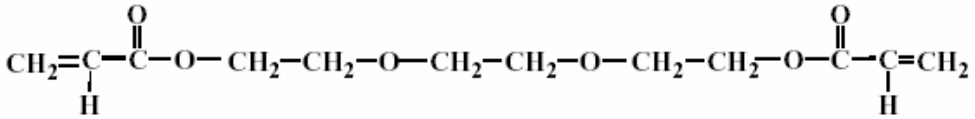

Since SR272 has only two carbon double bonds it forms less dense cross-linked networks compared to either SR351 or SR494. All monomers except for SR494 were used as received from Sartomer. A small amount of SR494 was deinhibited for experimental purposes. Table 4.1 provides a summary of important information for the above mentioned monomers. The critical degree of conversion required to induce gelation, the last column of Table 4.1, was calculated using the Flory definition of monomer functionality and Equation 2.23.

Table 4.1: Informational summary of acrylate monomers used in this investigation.

Acronym	Name	# of Functional Groups	Molecular Weight (g/mol)	Specific Gravity at 25° C	Refractive Index at 25°C	Critical Degree of Conversion
SR272	triethylene glycol diacrylate	2	258	1.109	1.461	0.333
SR351	trimethylolpropane triacrylate	3	296	1.109	1.472	0.200
SR494	ethoxylated pentaerythritol tetraacrylate	4	528	1.128	1.471	0.143

4.1.2 Photoinitiator

Since acrylate monomers are unable to produce free-radicals upon exposure to UV light, it is necessary to introduce a photoinitiator to the system. Ciba Irgacure 651, 2,2-dimethoxy-1,2-diphenylethan-1-one, is a general-purpose photoinitiator with the following chemical structure:

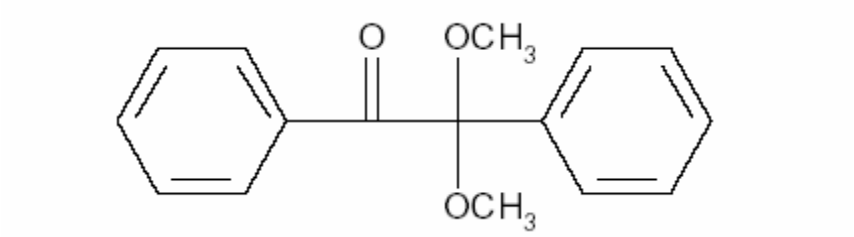

It was chosen for this investigation because it is highly efficient in curing unsaturated acrylate monomers. In addition, Irgacure 651 has good absorption spectra at the wavelengths of UV light used in this research. The absorption spectra are shown below in Figure 4.1. The absorbance value at a given wavelength indicates the ability of the photoinitiator to absorb photons at that wavelength; the higher the absorption, the better the photoinitiator is at absorbing photons.

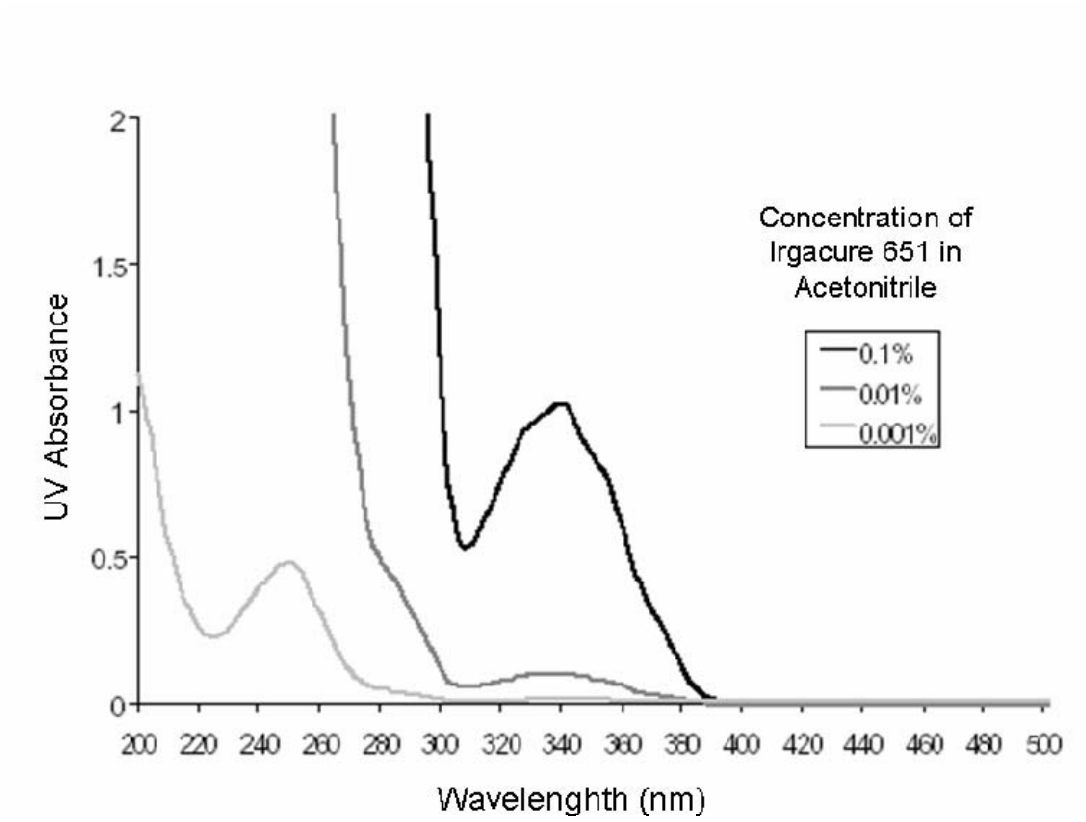

Figure 4.1: Absorption Spectra of Ciba Irgacure 651 at different concentrations in acetonitrile (Graph directly obtained from Ciba).

4.1.3 Fluorescent Tracer Particles

In order to track changes in the photopolymerization system with particle microrheology, micron sized, inert fluorescent tracer particles were obtained from a research group at the University of Twente, the Netherlands. The silica based particles contained red fluorescent dye (rhodamine) and have a diameter of 0.5 micron[46]. Silica particles were used instead of the more common polystyrene particles because the monomers under investigation leached the fluorescent dye by swelling the polystyrene particles.

The particles were stored in ethanol before being transferred to the monomer solution through a series of washing steps. A small quantity of ethanol/particle suspension was centrifuged at 3000 rpm for 30 seconds in an Eppendorf Mini Spin centrifuge. The ethanol supernatant was then removed and replaced with fresh ethanol for further washing to remove water impurities. This process was repeated two more times. This process is needed because water can affect the polymerization kinetics. After the third washing step, the ethanol supernatant was replaced with monomer. The particles were then washed three more times in pure monomer to remove the ethanol and obtain the final particle suspension.

4.1.4 Sample Preparation

In order to simplify sample preparation, a standard monomer solution containing 10 wt.% of initiator was prepared for each of the three monomers. The solid photoinitiator was weighed on a Mettler Toledo AG204 balance before the liquid monomer was added to obtain an initiator concentration of 10 wt.%. The solution was

then mixed using a Fisher Scientific Mini Vortexer and sonicated with a Fisher Scientific FS20H Sonicator. The standard solutions were then stored in a refrigerator until particle suspension and/or pure monomer was added to obtain the desired initiator and particle concentrations.

4.2 Experimental Design

The objective of this study was to use microrheology to perform in-situ monitoring of photopolymerization. In order to achieve this objective a sample chamber fitting the microscope had to be fabricated. In addition, a UV illumination setup had to be configured around the microscope.

4.2.1 Fabrication of Sample Chamber

Microrheology requires only a minute sample volume; therefore, a small, disposable sample chamber that was compatible with an inverted microscope was designed. The fabrication began with a Fisherbrand precleaned microscope slide. Two pieces of Parafilm M laboratory film, separated by a 1 mm gap, were placed in parallel on top of the glass slide. A Fisherbrand microscope cover glass (#1.5) was then centered and placed over the gap in the Parafilm. The stack of materials was then heated, causing the Parafilm to melt and adhere to both the cover slip and the glass slide, thereby creating a thin, open chamber capable of holding approximately 2 to 3 μL of sample.

The sample was loaded into the chamber using a micropipette and then the chamber was sealed with vacuum grease to prevent evaporation when necessary. In order to minimize the effects of shrinkage, a thin steel mask with a narrow slit was placed

perpendicular to the sample channel on the side of the microscope slide, leaving the cover slip side to face the microscope objective. The total sample area exposed to UV light was approximately one millimeter squared. Figure 4.2 provides a diagram of the designed sample chamber loaded with a sample. The transmission spectrum of the cover slide and the microscope slide are shown in Figure 4.3.

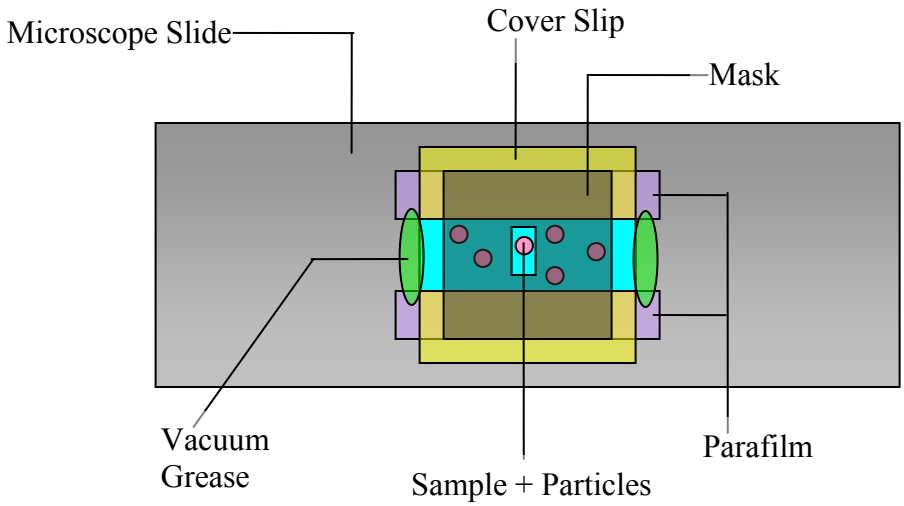

Figure 4.2: Schematic of fabricated sample chamber loaded with a sample.

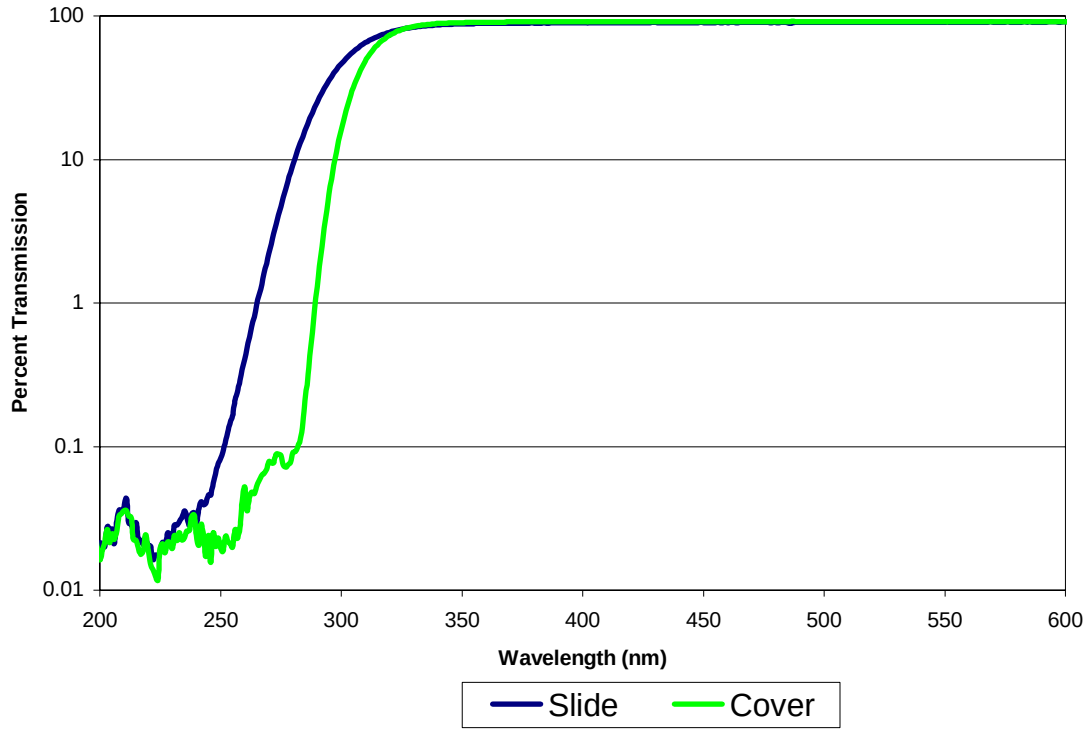

Figure 4.3: Transmission spectrum of glass cover slip and microscope slide.

4.2.2 Experimental Setup

The experimental setup was designed around a Leica DM-IRB inverted microscope set atop a Newport optical table. The microscope is equipped with four objectives (100x, 63x, 40x, and 10x) and two cameras, which are connected to a computer. The first camera is an analog 640 x 480 pixel CCD that has a frame rate of 30Hz (Cohu 4920). The second is the Hamamatsu EM-CCD Digital Camera C9100, which has a variable frame rate. A monitor was used to display the images taken by the Cohu analog camera. A high-speed Uniblitz VMM-D1 shutter was inserted in the microscope fluorescent light path to accurately control illumination. Located adjacent to the microscope was a Spectra-Physics arc lamp housing apparatus (model 66923) equipped with a 1000 watt Hg(Xe) UV lamp. Figure 4.4 provides the spectral irradiance

of the lamp. The lamp housing was raised off the table six inches using optical posts. A Spectra-Physics liquid filter was mounted in the UV light path directly in front of the condensing lens. The filter removed most of the IR spectra, while allowing the transmission of visible and UV light. A zero aperture iris diaphragm was mounted to the front of the liquid filter to control the illumination path of UV light. A Tech Spec First Surface mirror coated with enhanced aluminum was mounted on the opposite side of the microscope, directly across from the condensing lens of the lamp assembly. The mirror was set at 45° angle in order to divert the UV light path to the sample. Figure 4.5 provides a schematic drawing of the experimental setup.

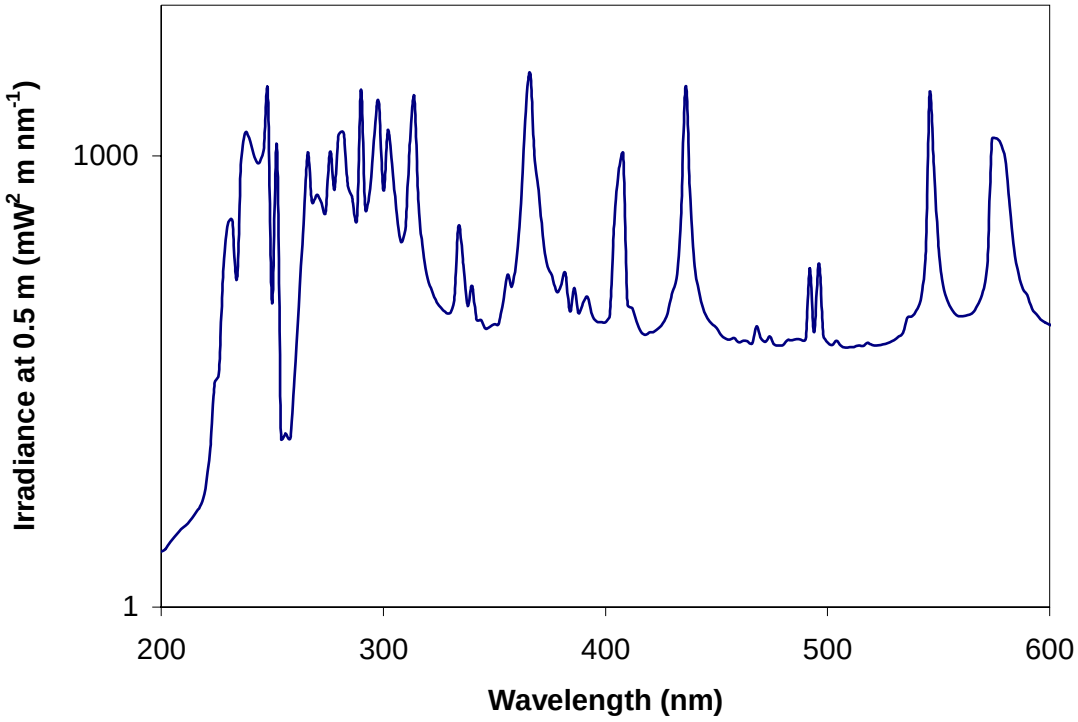

Figure 4.4: Spectral irradiance of 1000 W Hg(Xe) arc lamp.

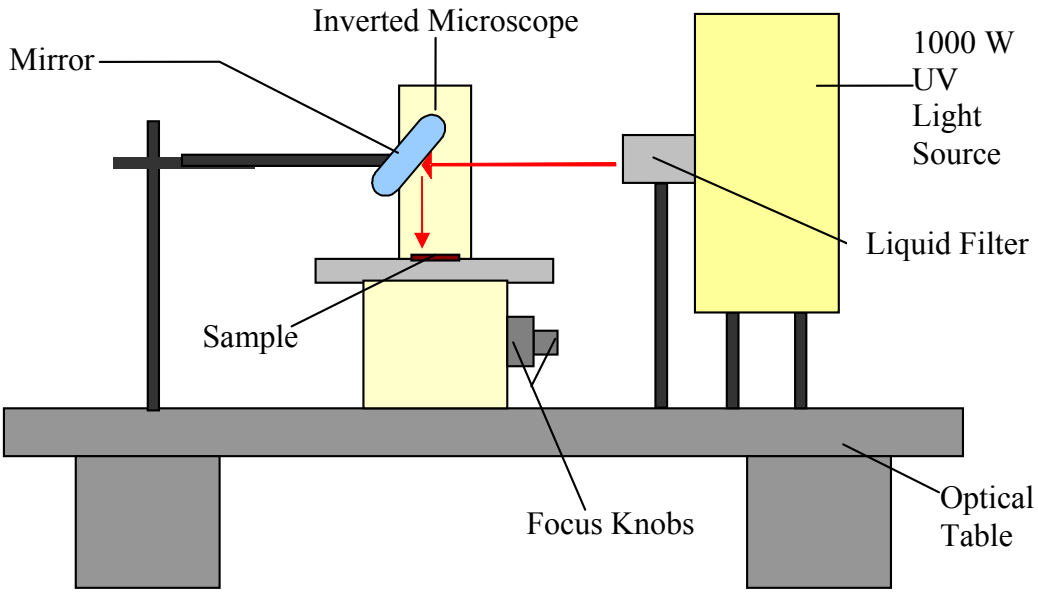

Figure 4.5: Schematic of the experimental setup.

4.2.3 Data Acquisition

The samples were loaded into the sample chamber and then placed on the microscope stage with the cover slip side of the chamber facing the 100x objective. The decision to employ the 100x oil-immersion objective was based on the size and concentration of the particles used. The sample was then positioned so that the one millimeter squared area, visible through the steel mask, was directly over the center of the objective. A detailed diagram of the alignment in the acquisition setup is shown in Figure 4.6. Various settings on both the camera and microscope were optimized to obtain maximum image quality for particle tracking.

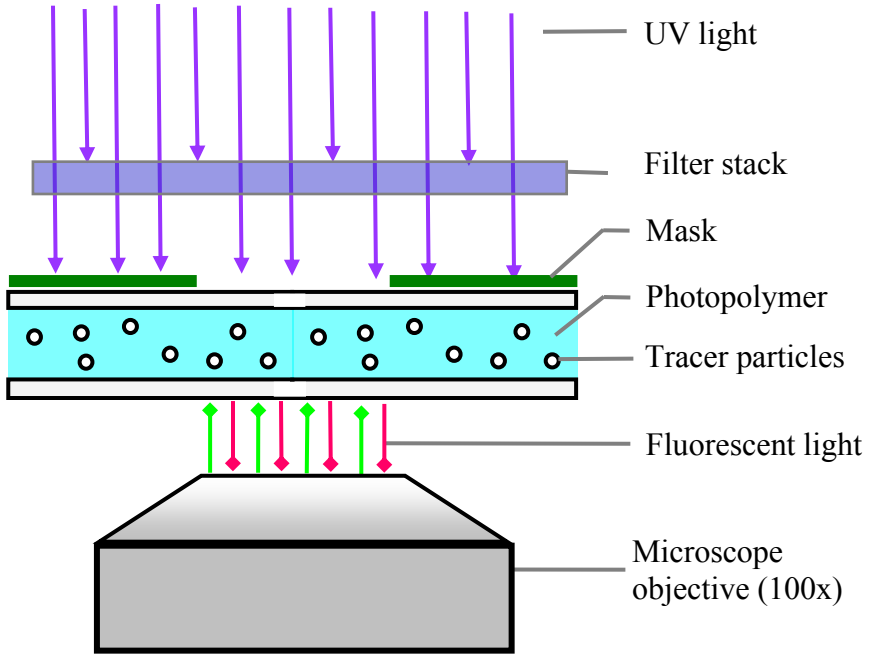

Figure 4.6: Schematic of data acquisition and experimental setup.

Images of the fluorescent tracer particles were transferred to the computer and recorded in real-time using PXC-200, a precision frame grabber, and OpenBox, specialized image acquisition software. After a predetermined number of images were recorded, the iris diaphragm on the UV light path was opened and the polymerization process was initiated. After completion of the image acquisition, OpenBox was used to divide the video file into a series of image stacks for further analysis.

4.2.4 System Parameters

The designed experimental setup allowed for the variation of several parameters. The effects of varying the wavelength and intensity of UV light, UV penetration depth, and concentration of inhibitor on the gelation process were studied. The effects of oxygen inhibition were also examined.

4.2.4.1 Wavelength of UV Light

Two different wavelengths of UV light were investigated: 248 nm and 356 nm. The wavelength of UV light was varied using UV bandpass filters. The 248 nm UV bandpass filter had a 30 nm bandwidth and was obtained from Barr Associates. Newport supplied the 356 nm UV bandpass filter, which had a bandwidth of 30 nm. The transmission spectra of the 248 nm and 356 nm filters are shown in Figure 4.7.

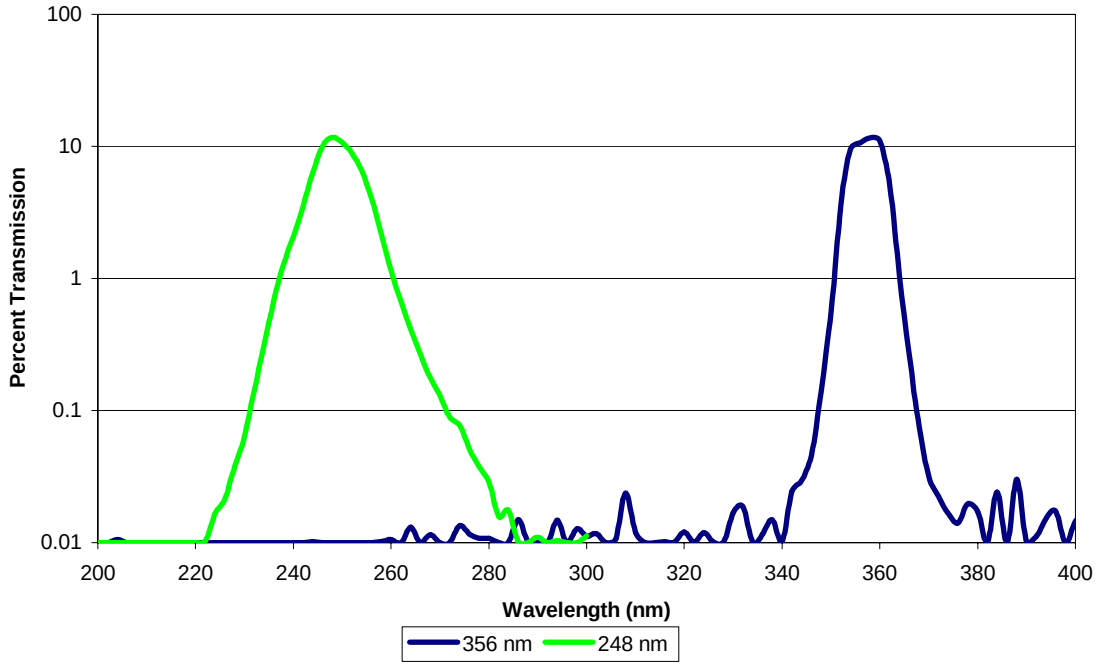

Figure 4.7: Transmission spectrum of 248nm UV bandpass filter and 356 nm UV bandpass filter.

4.2.4.2 Intensity of UV Light

The intensity of UV light transmitted to the sample with both the 248 nm and 356 nm bandpass filters was measured in (mW/cm^2) using a Molectron EPM 2000e Dual-Channel power meter. The intensity at both wavelengths was varied using neutral density

filters obtained from Newport. The filters used are shown in Figure 4.8 , the filters are classified by optical density: 1.0 OD (ND10), 0.3 OD (ND03), and 0.1 OD (ND01). The transmission spectra of the 1.0 OD, 0.3 OD, and 0.1 OD neutral density filters are shown in Figure 4.8. For the experimental procedure, the neutral density filters were stacked on top of the bandpass filters and placed in the path of the UV light. The unfiltered intensities were measured using the power meter, while the filtered intensities were calculated by multiplying the unfiltered intensity by the fraction of light transmitted by the neutral density filter at that appropriate wavelength. Table 4.2 lists the measured and calculated intensity of UV light received by the sample.

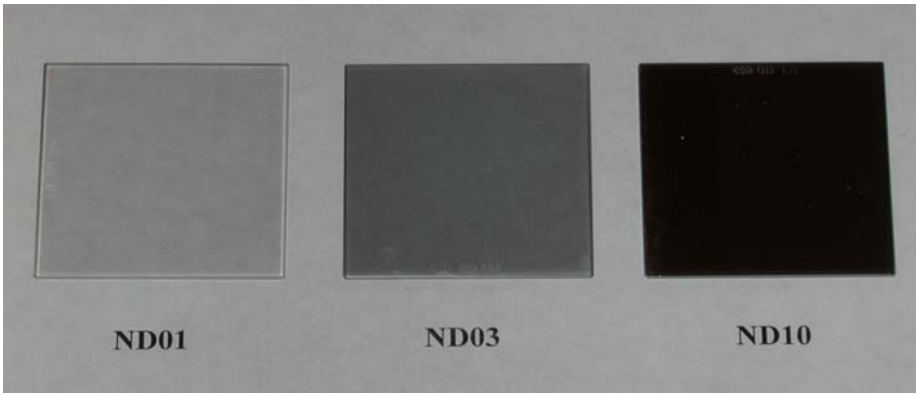

Figure 4.8: Picture of neutral density filters.

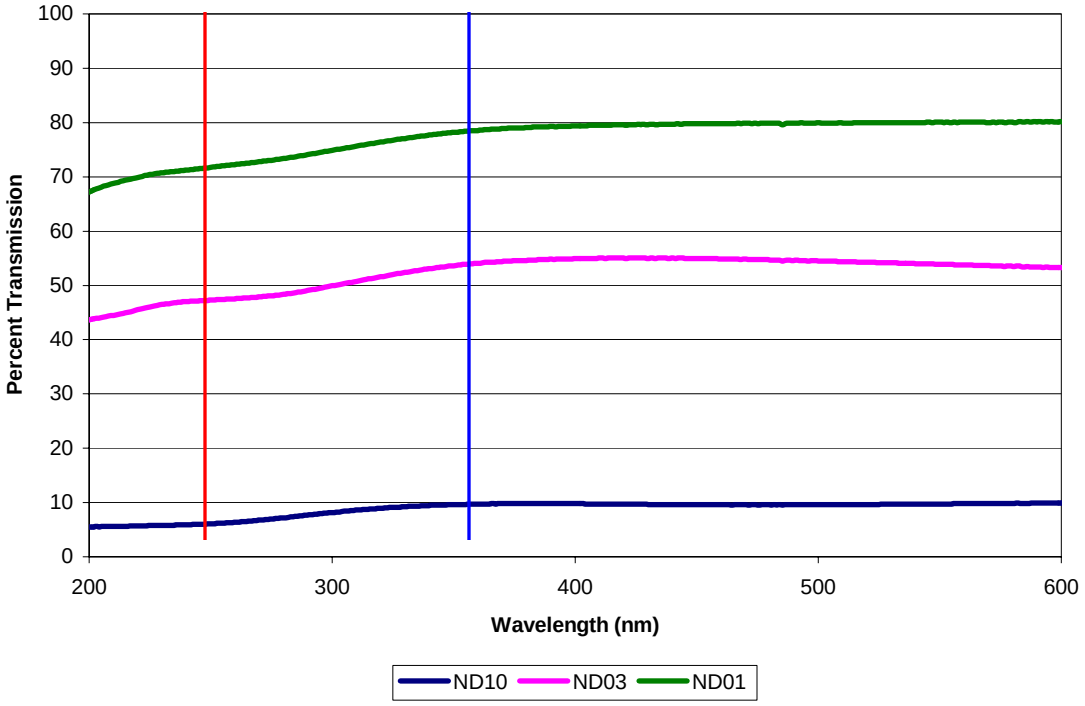

Figure 4.9: Transmission spectrum of ND01, ND03, and ND10 neutral density filters. The red vertical line is at 248 nm and the blue line is at 356 nm.

Table 4.2: Measured intensity of UV light at 248 nm and 356 nm using filters with various optical densities.

	248 nm (mW/cm^2)	**356 nm (mW/cm^2)**
Unfiltered	**0.0063**	**0.4000**
ND10	**0.0004**	**0.0387**
ND03	**0.0027**	**0.2116**
ND01	**0.0045**	**0.3137**

4.2.4.3 Location in Sample

The thickness of the sample was measured from the top illuminated surface to the bottom surface using the fine focus wheel on the microscope. It was known that for each measurement unit on the fine focus wheel the actual distance was 2 microns. The top of the sample was then defined as $D = 0$ (see Figure 4.10) and any location in the sample was thereafter defined as distance from the illuminated surface to the focal plane. The

depth of the focus (thickness of the focal plane shown in Figure 4.10) was estimated to be 1-2 μm by moving the fine focus knob of the microscope. As a result, the distance over which the particles in an image can move in the out-of-plane direction and still be recorded is 1-2 μm.

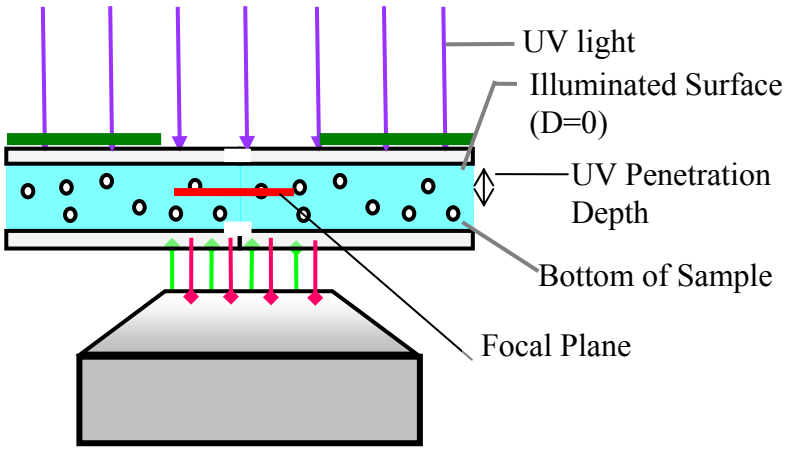

Figure 4.10: Illustration of sample depth.

4.2.4.4 Addition of Inhibitor

The monomer samples received from Sartomer contain a small amount of inhibitor, either 8-Hydroxyquinoline (HQ) or 4-Methoxyphenol (MEHQ), to prevent prepolymerization. The sample of SR494 was shipped with approximately 240 ppm of MEHQ. To test the effects of inhibitor on polymerization, a small amount of SR494 was deinhibited by the research group of Professor Henderson. MEHQ, used as obtained from Aldrich, was then added to the deinhibited sample to create a range of concentrations. The chemical structure of MEHQ is:

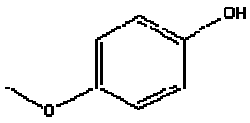

The concentrations investigated in this experiment were: 0, 250, 500, and 1000 parts per million by weight.

4.2.4.5 Deoxygenation

Since the experimental system could not be blanketed with an inert gas, the sample had to be degassed and loaded into the sample chamber in an oxygen-free environment in order for the effects of oxygen inhibition to be studied. The research group of Professor Jones degassed the sample under vacuum and placed it in a glove box. The sample was loaded into the sample chamber and sealed with vacuum grease while inside the glove box. Upon removal from the glove box, exposure of the sample to light was minimized and the microrheology experiment was immediately run in order to prevent early polymerization and reoxygenation of the sample.

4.3 Analytical Procedure

Statistical analysis of the Brownian motion of the tracer particles can be used to extract rheological information about the embedding medium as a function of time and space. This data can then be used to relate UV exposure to the polymerization and gelation of monomeric resins.

4.3.1 IDL

Interactive Data Language (IDL) is a proprietary software system distributed by Research Systems, Inc. The software was first used by NASA but has since become a common computer programming language used by scientist and engineers. IDL is employed in this work to perform the image and statistical analysis that is used to translate tracer particle motion into rheological properties. The accuracy of using IDL to perform statistical analysis of particle motion has been well established; as a result, it is the preferred analysis method of microrheological research. The IDL analysis consists of three main steps: location of the particle positions in every frame of the movie, linkage of the particle positions among successive frames to form trajectories, and the determination of the MSDs[47]. The main weakness of using IDL is that the statistical results can be sensitive to the initially chosen parameters; however, these effects can be virtually eliminated with experience.

Once the full length videos are broken down into stacks of images, statistical analysis of particle motion can be performed by IDL. Since some images may contain particles that are either indistinguishable from the background or part of aggregates, the particle detection step requires that images be processed with a series of filters. In order to improve statistics, particle selection is optimized by placing limitations on certain parameters such as particle size, average brightness, and elongation. The parameter limitations and filter settings are chosen based upon the size of particles and magnification of the optical setup that was used to create the images. This elaborate process can either be done in a step-by-step process for each image or by writing a program that combines all the steps into one process. For analysis in this research the

programs *PRE_ANALYZE.PRO* and *TIFF_PRETRACK.PRO*, were used to simplify the process[47]. *PRE_ANALYZE.PRO* (originally coded by V. Breedveld) allows for the interactive determination of the optimal filter and parameter limits, while *TIFF_PRETRACK.PRO* (originally coded by J. Crocker) uses the chosen parameter settings to analyze all image stacks of a single movie. Once the particle positions have been determined, the program *TRACK.PRO* (originally coded by J. Crocker) is used to stitch the images together and identify the particle trajectories as a function of time[47].

Data files created by *TRACK.PRO* that contain motion and trajectory information can be transformed into MSD data using *MSD_TIME.PRO* (originally coded by V. Breedveld). The Brownian motion of the particles is expected to yield random displacements with Gaussian distributions. If there is significant deviation of the data from the Gaussian fit, MSD cannot be accurately determined and the system has to be reparameterized[47]. The program outputs an array that contains data such as frame number, lag time, and MSD. The data can then be analyzed further to produce graphs of MSD as a function of frame number (real time) and lag time.

4.3.2 Definition of Gel Point with Microrheology

The classic Winter—Chambon criteria, which states that the loss tangent becomes independent of frequency at the gel point[30], could not be applied in this research since frequency is unable to be varied in passive microrheology. A theoretically equivalent definition of the point of gelation is the loss and storage modulus being congruent and proportional to the frequency ($G' \sim G'' \sim \omega^{1/2}$). The congruence definition is consistent with the Kramers-Kronig relation; therefore, the loss and storage modulus being equivalent is

just as much a rheological property at the gel point as are infinite viscosity and zero equilibrium modulus. A slope of 0.5 in a double-logarithmic plot corresponds to $\langle \Delta r^2(\tau) \rangle \sim \tau^{1/2}$, which can be derived from the congruence definition of $G' \sim G'' \sim \omega^{1/2}$. As a result, the gel point can be determined graphically in microrheology by plotting the slope of the MSD curve as a function of time. The time at which the transient slope profile is equal to a value of 0.5 is determined to be the gel point.

CHAPTER 5

RESULTS AND DISCUSSION

In this chapter, the experimental results will be presented and discussed in four sections: proof of concept results, depth profiling, intensity and Beer's law, and kinetics. This research project is the first known attempt in which microrheology is used as a technique to study photopolymerization; comparisons will be made to results obtained with other techniques when appropriate. The results are intended to show the unique capabilities of microrheology to perform in-situ monitoring of photopolymerization.

5.1 Proof of Concept Results

The first experiments were performed on SR494 loaded with 5.0 wt.% photoinitiator to evaluate the ability of microrheology to distinguish between a liquid sample and a photopolymerized gel. The motion of particles in two samples of SR494, one of which had been exposed to UV light for approximately 100 s, was tracked and statistically analyzed. Figure 5.1 shows the plot of MSD as a function of lag time for these preliminary experiments. As illustrated in Figure 5.1, microrheology is without a doubt capable of distinguishing between the exposed and unexposed samples. The MSDs of the exposed and unexposed samples differ by several orders of magnitude. The exposed sample has a slope of zero in the double-logarithmic plot of MSD versus lag time, while the unexposed sample has a slope of one. These slopes are characteristics of

an elastic gel and a viscous Newtonian liquid, respectively. For the unexposed liquid sample, the MSD increases with time, as seen in Equation 3.1, since the particles are able to move freely, while the particles in the exposed gel sample are trapped in the dense cross-linked network, and therefore, the MSD remains constant, as illustrated by Equation 3.2. Since the unexposed sample in Figure 5.1 is a textbook example of a Newtonian fluid, it can be inferred that the fluorescence light of the microscope does not contribute to mechanical changes in the sample.

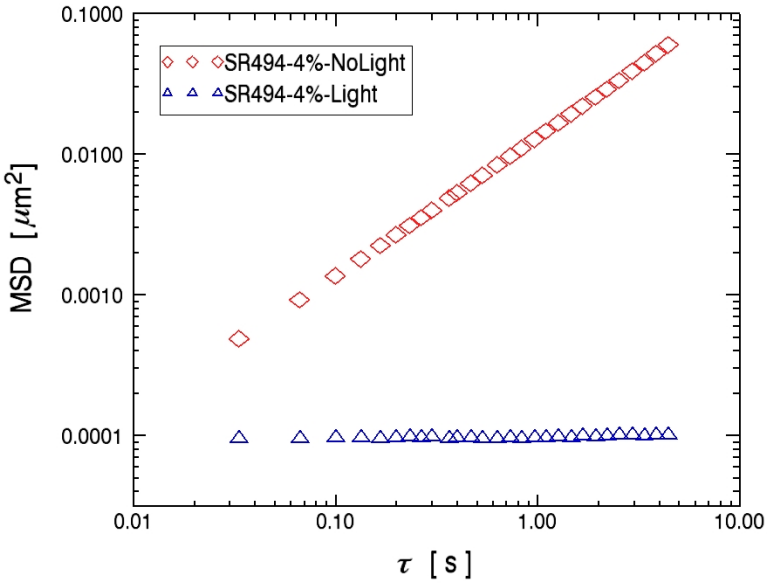

Figure 5.1: MSD of tracer particles as a function of lag time for SR494 with 5.0 wt% photoinitiator.

Next, a similarly prepared sample of SR494 was used to prove the ability of microrheology to perform in-situ monitoring of the progress of photo-induced polymerization. Using the experimental setup described in Chapter 4, the sample was exposed to UV light after 200 frames (6.6 s) by a manually controlled shutter. Figure 5.2 shows the real-time development of the MSD profile for the exposed resin. The MSD is

only presented for the three shortest lag times in order to maximize temporal resolution. The three shortest lag times (33ms, 67ms, and 100ms) are equivalent to the first three data points of Figure 5.1, as shown in inset of Figure 5.2. The transient MSD curves show that microrheology can accurately be used to monitor changes in sample rheology of photoresins exposed to UV light. Before the liquid-to-solid transition the MSD increases with increasing lag times, a characteristic of a viscous liquid. The independence of the MSD on the value of lag time after the transition is a characteristic of an elastic gel. In addition, Figure 5.2 illustrates a significant delay time before exposure to UV causes photoresins to form a polymerized gel. The spikes in the transient MSD curves of Figure 5.2 around 200 images are a result of vibrations of the system caused by the opening of the primitive shutter.

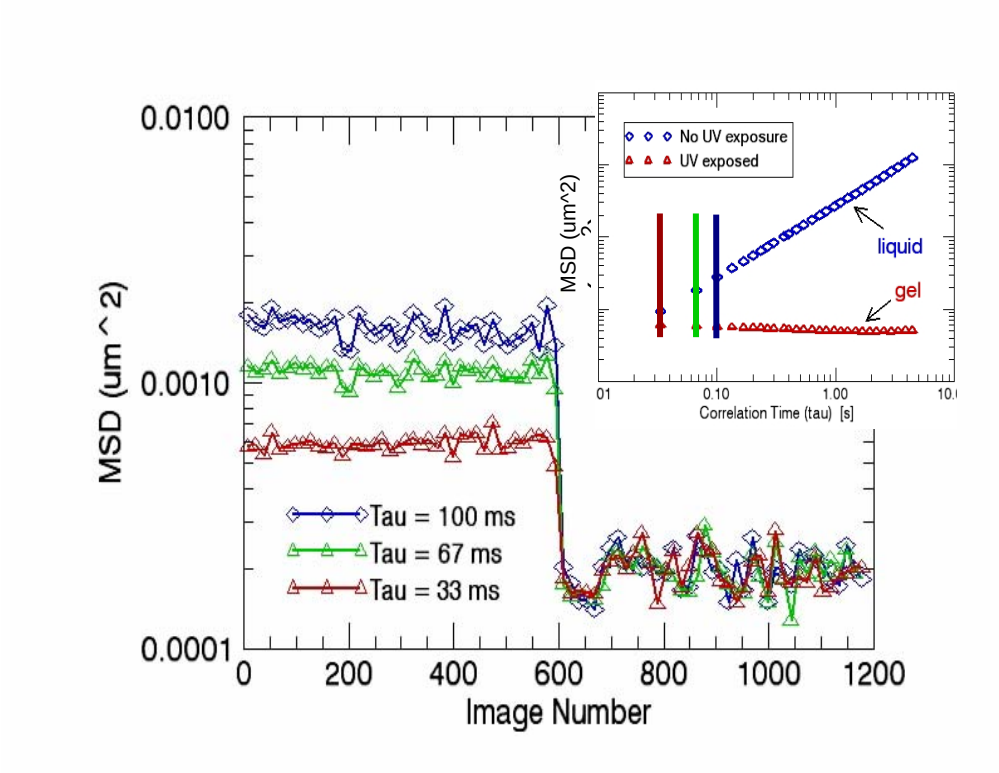

Figure 5.2: Transient MSD for tracer particles in a curing sample of SR494 loaded with 5.0 wt% photoinitiator. The inset illustrates how the corresponding figure can be interpreted in terms of gels and liquids. Gelation occurs at image number 590.

In order to determine the point of gelation, the slope of the transient MSD curves verses lag time were plotted as a function of time. The MSD curves for three different lag times (67ms, 100ms, and 133ms) were used to obtain the actual transient slope for MSD versus lag time as a function of time. The shortest lag time, which is often imprecise because of insufficient spatial resolution of the particle detection, was not used to improve statistics. The transient slope for a sample of SR494 loaded with 5.0 wt.% photoinitiator is shown in Figure 5.3. This data corresponds to the transient MSD profile shown in Figure 5.2. It can clearly be seen by examining the slope profile in Figure 5.3, that the data can be modeled using a sigmoidal fitting curve. A simple sigmoid fit was applied with four parameters:

$$y = \frac{m1 + m2}{1 + \exp\left(-\left(\frac{x - m3}{m4}\right)\right)} \tag{5.1}$$

where x is the value of the x-axis, *m1* is the y-axis value of the sigmoidal curve after the drop, *m2* is the magnitude of the sigmodial drop, *m3* is the midpoint, and *m4* is the duration of the sigmoidal transition. The slope profile in Figure 5.3 does not begin and end at the theoretically predicted values of one and zero, for a liquid and gel respectively, because of spatial resolution limitations and statistical noise. Since the data in Figure 5.2 has such a rapid decline in MSD around image number 600, there are virtually no data points in the descending region of the fitting curve shown below.

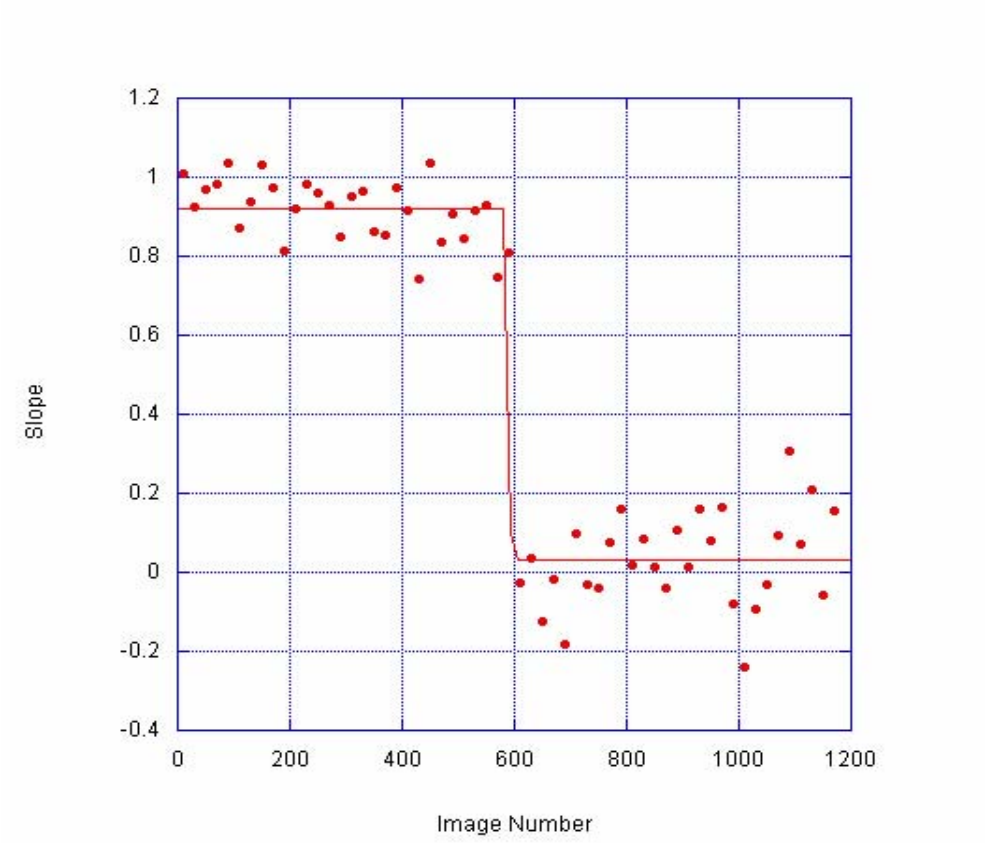

Figure 5.3: Graph of slope value vs. image number. The data was fitted to a sigmoidal curve. Gel point occurs when slope is equal to 0.5 (i.e., approximately at image number 592).

Based upon the Winter-Criterion gelation theory[30] first introduced in Section 2.5 and later theoretically expand to the method of microrheology in Section 4.3.2, the midpoint of the sigmoid fit used in Figure 5.3 is equivalent to a slope value of 0.5 and can therefore be used as the definition of gel point. According to this definition, the gel point occurs at image number 592, which is nearly the same time that the MSD curves become independent of lag time in Figure 5.2. Consequently, the point at which the MSD curves first collapse upon each other can also be used to define the gel point. Figures 5.2 and 5.3 clearly illustrate that the two methods for determining the gel point

using microrheology are equivalent; as a result, the method illustrated in Figure 5.2 will be employed for the analysis of all results.

A final basic experiment was performed on a sample of SR351 loaded with 1.0 wt% of photoinitiator to explore the spatial resolution of the microrheological setup. The sample was masked in order to reduce shrinkage by limiting the area exposed to UV light. After the sample was allowed to cure for approximately 1 minute, UV illumination was terminated and measurements of microrheology were performed at the edge of the masked area. SR351 was selected for this experiment instead of SR494 because the lower viscosity of SR351 results in increased particle motion, making it easier to detect the solid-liquid phase boundary in the masked sample. The resulting curves of MSD as a function of position are shown in Figure 5.4. The inset shows the full trajectories of all tracer particles in the field of view. From the trajectories, it is clear that the particles to the right of the phase boundary are unable to move because they are trapped in the cross-linked gel network, while the tracer particles to the left of the boundary are able to diffuse without constraint. The observation is clearly supported by the MSD data in Figure 5.4. On the left side of Figure 5.4 the transient MSD curves depend on lag time, which is a characteristic of a viscous liquid, while on the right the MSD is independent of lag time, indicating a gel. Inspection of the proof-of-concept results clearly reveals the unique capabilities of microrheology to perform in-situ monitoring of free-radical photopolymerization.

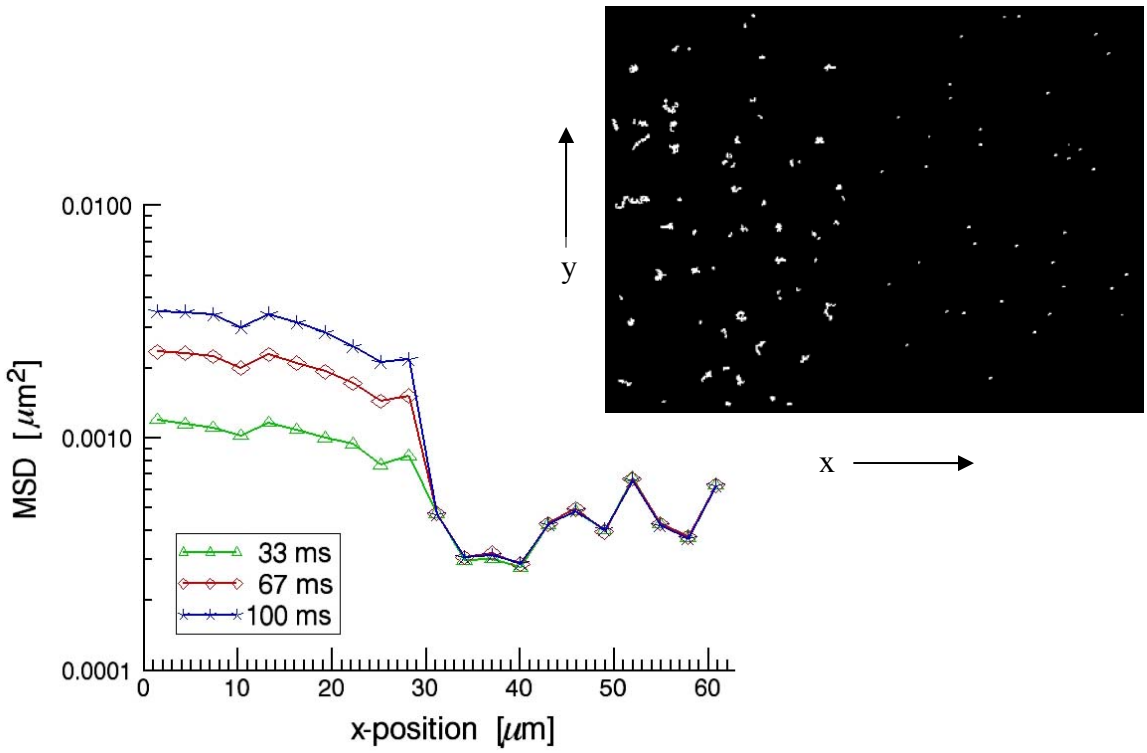

Figure 5.4: Spatial variations of tracer particle MSD in a partly exposed cured sample of SR351 loaded with 1.0 wt% photoinitiator.

5.2 Depth Profiling

The initial results show that microrheology is suitable for tracking rheological changes in photoresins as a function of time and location within the two-dimensional focal plane. The experimental setup shown in Figure 4.5, however, also allows accurate positioning of the focal plane in three-dimensional space by varying the location of the focal plane as shown in Figure 4.10. Microrheology was used in this project to study the homogeneity of gelation as a function of UV penetration depth. Initially, a sample of SR494 loaded with 5 wt% photoinitiator was masked and exposed to UV illumination at either 248 nm or 356 nm after approximately 200 images. The depth at which the movies were taken, was varied using the fine focus knob of the microscope over the entire thickness of the sample chamber, which was approximately 120 micrometers. The top

surface of the sample chamber was defined as the point of zero UV penetration depth; all other UV penetration depths were defined as the distance from this top surface.

The plots of gelation time versus UV penetration depth are shown in Figure 5.5 for a sample of SR494 loaded with 5.0 wt% photoinitiator exposed to 248 nm and 356 nm UV light. Figure 5.5 clearly shows a significant variation in gelation time across a 100 μm sample. A factor of three increase in gel time was observed as the focal plane was varied from the top to the bottom of the sample chamber. The significant difference in gel time as a function of UV penetration depth can at least partly be explained with Beer's Law, Equation 2.4. Beer's law describes the exponential decay of the amount of photons delivered to the sample with increasing thickness of the absorbing medium. In essence, the top of the sample is exposed to a larger fraction of incident light than the bottom. As a result, the photoinitiator near the top of the sample will absorb a greater amount of photons, thereby increasing the production of free-radicals, and ultimately rate of polymerization. The greater absorption of photons at the top of the sample limits the initiation reactions of free-radical photopolymerization, shown in Equations 2.13-2.14, deeper into the sample.

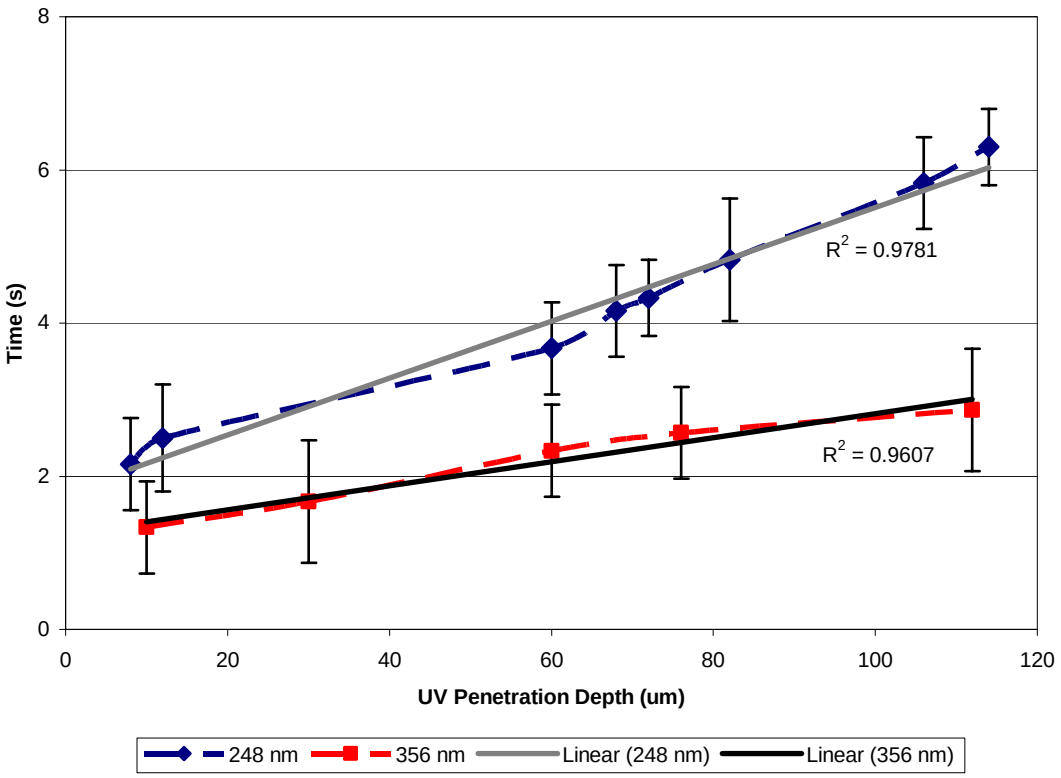

Figure 5.5: Plot of gelation time as a function of UV penetration depth for SR494 loaded with 5.0 wt% photoinitiator cured using both 248 nm and 356 nm UV irradiation

The error bars in Figure 5.5 are mainly a result of the use of a primitive shutter to control the illumination of UV light. As illustrated in Figure 5.2, the photoresin sample is kept in the dark for approximately 6.6 seconds (200 images) before being exposed to UV light. Because exposure to UV light is controlled by a simple iris diaphragm and not an electronically controlled shutter, the exact time at which UV exposure occurs is difficult to determine. Opening the iris diaphragm causes small vibrations of the sample on the microscope stage; the time over which these vibrations occur (usually less than 0.5 seconds) is considered the error in initially exposure time. Determining the exact moment of gelation generates an additional error; however, this error is less significant than the error associated with the initial exposure time. The initial exposure time error

and the error in gelation time were combined to determine the total error in the system, which is shown in all figures where gelation time is measured. To determine the reproducibility of the data obtained from the designed setup several experiments were conducted at the same location. The gel point at given location was considered reproducible since all of the experimental data overlapped within a margin of error less than 5.0 %. The reproducibility error was often smaller than the error assigned to individual measurements.

Another explanation for the increase in gelation time across the sample layer is the possible decrease in the transmission of UV light caused by the early gelation of the illuminated surface. Once the top of the sample reaches a critical degree of polymerization, the UV light has to penetrate two phases: solid and liquid polymer. The gelation process is expected to affect the optical properties of the polymer such as refractive index, which could lead to a decrease in the intensity of UV light transmitted to remaining liquid polymer. This explanation would require a non-linear dependence of UV penetration depth on gelation time would be expected. Several fitting curves, such as linear, exponential, and power, were applied to the data in Figure 5.5. Of all the applied fitting curves the linear model consistently had the R^2 value closest to unity. By definition, R^2 is the fraction of the total squared error that is explained by the model. Although the R^2 value is not an absolute determinate of best fit, it does proved insight into the predictive power of the applied model. The fact that the curves in Figure 5.5 can be best described as linear challenges the above explanation.

Figure 5.5 shows that a sample exposed to constant UV illumination at 248 nm takes twice as long to gel when compared to the same sample exposed at 356 nm. This

may at first seem counterintuitive since 248 nm UV light contains more energy than 356 nm UV light. The amount of that energy, however, that is actually transmitted is the ultimately determining factor. Before reaching the sample, the filtered UV light must pass through a Fisherbrand glass microscope slide. As seen the transmission spectrum of the glass slide shown in Figure 4.2 only 0.064% of the energy is being transmitted to the sample at 248 nm opposed to 88.4% at 356 nm. This is without a doubt the reason that gelation of SR494 loaded with 5.0 wt.% photoinitiator takes longer to occur at 248 nm. It is hypothesized that if the sample were to be illuminated without glass, the polymer would reach the critical degree of polymerization faster at 248 nm. Since nearly all of the energy at 248 nm is filtered by the glass used in the designed sample chamber the majority of the subsequent research will employ 356 nm UV irradiance.

The next step was to determine if the linear dependence of gelation time on UV penetration depth seen in Figure 5.5 was true for monomers of different functionality. Samples of SR272 and SR351 loaded with 5.0 wt.% photoinitiator were cured using 356 nm UV irradiance and compared to the results obtained using SR494. The results shown in Figure 5.6 confirm that the linear trend observed for SR494 is independent of functionality. An approximate factor of three difference in the gelation time from top to bottom was observed for all three monomers.

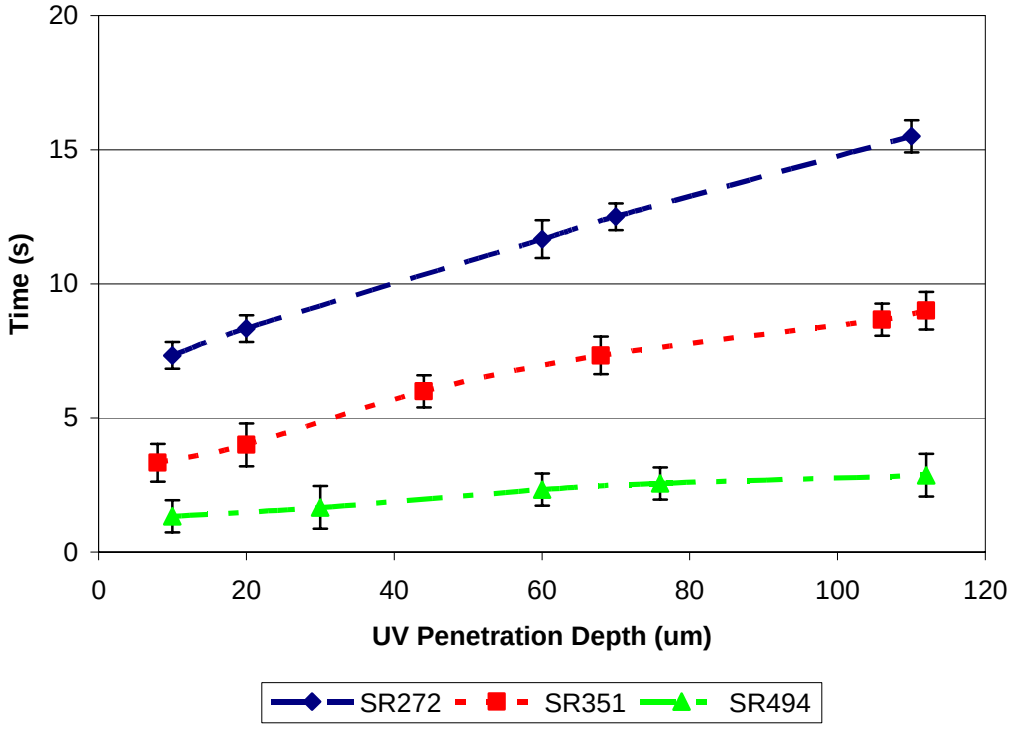

Figure 5.6: Plot of gelation time as a function of UV penetration depth for three different acrylate monomers: SR272, SR351, and SR494. All samples were loaded with 5.0 wt% photoinitiator and cured using 356 nm UV irradiation.

As illustrated in Figure 5.6, SR494 forms a gel faster than either SR272 or SR351 under the same illumination conditions, a result of SR494 having a higher functionality. Table 4.1 lists the functionality and critical degrees of conversion predicted by Flory for SR272, SR351 and SR494. Higher functional monomers form densely cross-linked networks more rapidly, and therefore, require a lower critical conversion threshold to induce gelation. The severe mobility restrictions imposed by cross-linking tend to change propagation and termination reactions mechanisms, shown in Equations 2.15-2.17, to diffusion controlled processes, resulting in lower overall conversion in higher functional monomers. Since SR494 has the highest functionality and lowest critical degree of conversion it makes sense that SR494 would gel first since it is more reactive.

The data shown in Figure 5.6 correspond to the theoretically prediction that lowest functional monomer, SR272, should be the slowest to form a gel.

5.3 Intensity Effects and Beer's Law

According to Beer's Law, increasing the intensity of UV light delivered to the sample should ultimately lead to a faster rate of polymerization. In this research, neutral density filters were used to investigate the effect of intensity on gelation time. Samples of SR494 loaded with 5.0 wt% photoinitiator were exposed to neutral density-filtered UV light at 248 nm and 356 nm. The experimentally determined intensity of the unfiltered and neutral density-filtered UV light at each wavelength can be found in Table 4.2 of the experimental chapter. Gelation results are shown as a function of UV penetration depth in Figures 5.7 and 5.8.

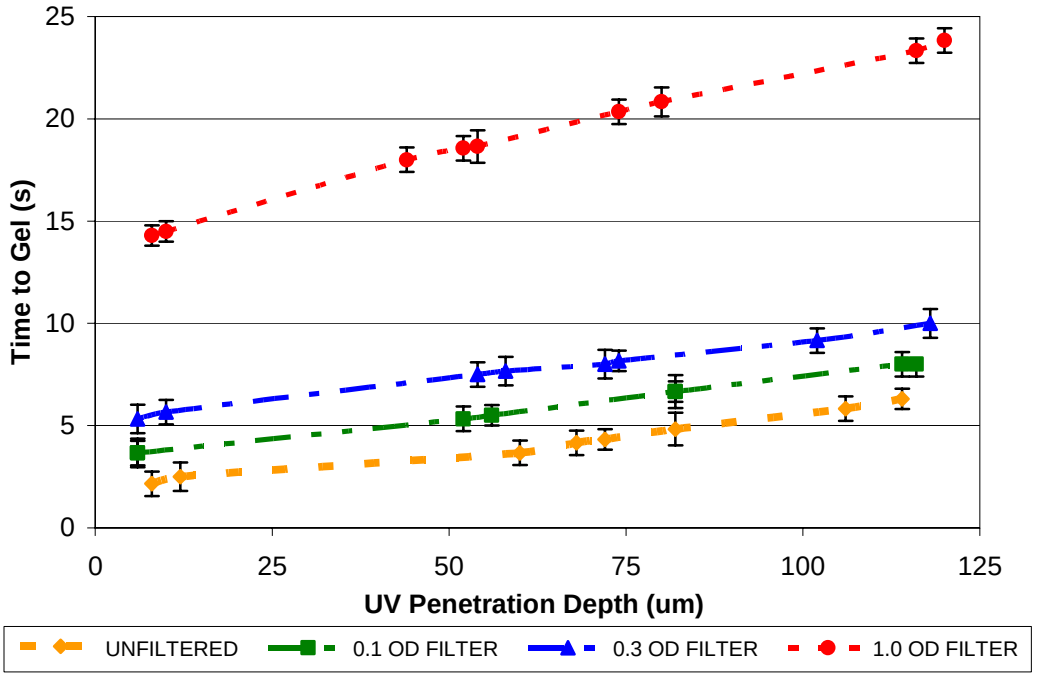

Figure 5.7: Plot of gelation time as a function of UV penetration depth and Intensity for SR494 loaded with 5.0 wt% photoinitiator cured using 248 nm UV irradiance.

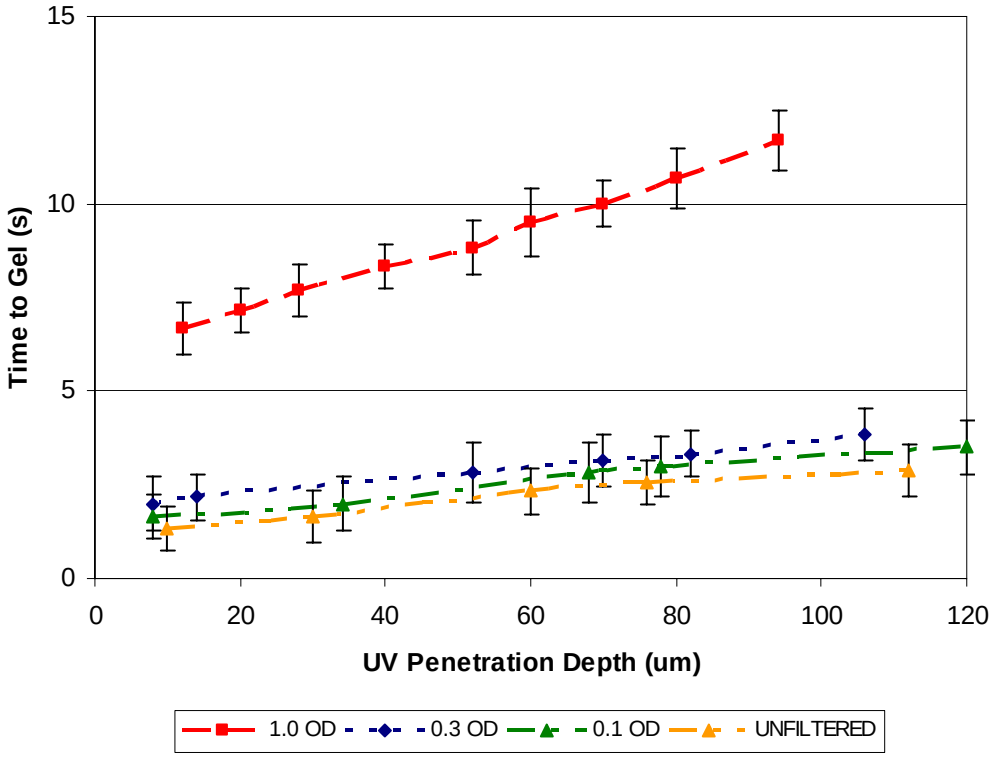

Figure 5.8: Plot of gelation time as a function of UV penetration depth and Intensity for SR494 loaded with 5.0 wt% photoinitiator cured using 356 nm UV irradiance.

As expected, using neutral density filters to decrease the intensity of UV light considerably increased the required gelation time. The intensity of UV light delivered to the sample primarily influences the initiation step, Equations 2.13 and 2.14, of the polymerization kinetics. Since free-radicals, which initiate polymerization, are formed by photochemical decomposition of initiator, the ability to cure a photoresin depends on the light intensity at a given depth in the sample. The rate of initiation of free-radicals at a depth x is given by the following equation[48]:

$$R_i = \varphi I_0 \varepsilon [In] \exp(-\varepsilon [In] x) \qquad (5.2)$$

where I_0, is the initial light intensity at $x = 0$, φ is the quantum yield for radical production, and *[In]* is the concentration of initiator with molar absorption coefficient ε. It is clear from the above equation that increasing the intensity of UV light leads to an increased generation of free radicals. The rise in the rate of initiation results in a faster gelation time.

The fact that the 248 nm samples are only approximately two times slower in gelation time compared to 365 nm may seem remarkable considering the comparison of the actual measured intensities of UV light shown in Table 4.2. This result, however, can partly be explained by the absorption curve of the Ciba Irgacure 651 photoinitiator shown in Figure 4.1 of the experimental chapter. By examining this graph it is clear that the absorbance of the photoinitiator at 248 nm is over 30 times greater than the value at 356 nm. The higher absorbance value suggest that at a given intensity a greater number of photons can be absorbed by the photoinitiator at 248 nm compared to 356 nm. Numerous studies have been performed that corroborate the trend illustrated in Figures 5.7 and 5.8 by showing that increasing the intensity of UV irradiance increases the curing speed[24, 25, 48-50].

Beer's law is often used to empirically predict the outcome of photopolymerization. A popular model assumption is that gelation occurs once a critical energy threshold, E_{cr}, has been reached. That energy threshold model is directly related to the intensity of UV light and gelation time by the following equation:

$$E_{cr} = I_a t_{gel} \tag{5.3}$$

As a result, the gelation time should approximately scale with the inverse of intensity delivered to a given location:

$$t_{gel} \sim \frac{1}{I_0 \exp(-kx)} \tag{5.4}$$

where the intensity delivered to a given location is defined according to Beer's Law, shown in Equation 2.4. The data in Figures 5.7 and 5.8 can be used to verify the accuracy of the empirical threshold model. Since both the material and location are constant between experiments, the exponential term in Equation 5.4 remains constant; therefore, gelation time should simply scale with the inverse of incident intensity, I_0, a known value. As a result the gelation time for experiments with neutral density filters should be given by:

$$t_{gel,\,filtered} = t_{gel,unfiltered}\left(\frac{I_{0,unfiltered}}{I_{0,\,filtered}}\right) \tag{5.5}$$

where $I_{0,filtered}/I_{0,unfiltered}$ is equal to the transmitted fraction of the neutral density filters, since all other elements in the experimental system remain the same. The results of normalizing the experimentally determined filtered gelation times to predicted unfiltered gelation times would provide insight into the validity of using empirical threshold model to predict of gelation. If renormalization of the filtered data in Figures 5.7 and 5.8 causes the curves to collapse, the accuracy of using threshold model is validated. The renormalized filtered-to-unfiltered gelation time is defined as:

$$t_{gel,norm} = t_{gel,\,filtered}\left(\frac{I_{0,\,filtered}}{I_{0,unfiltered}}\right) \tag{5.6}$$

where $t_{gel,\,norm}$ is the normalized time, $t_{gel,\,filtered}$ is the original time shown in Figures 5.7 and 5.8. The renormalization results are shown in below in Figures 5.9 and 5.10.

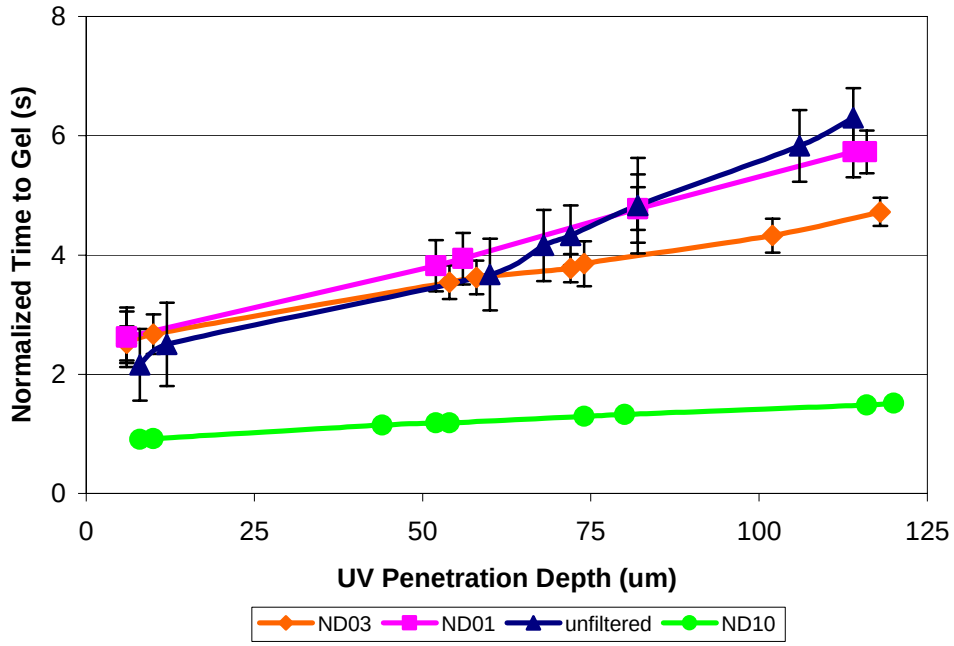

Figure 5.9: Plot of gelation time normalized to the unfiltered UV intensity as a function of UV penetration depth and Intensity for SR494 loaded with 5.0 wt% photoinitiator cured using 248 nm UV irradiance.

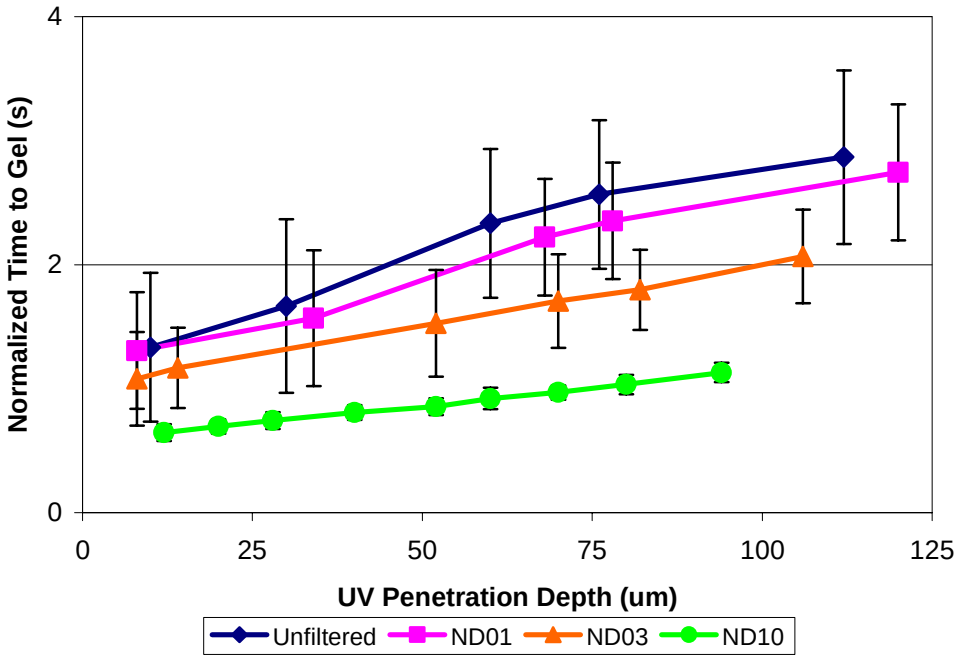

Figure 5.10: Plot of gelation time normalized to the unfiltered UV intensity as a function of UV penetration depth and Intensity for SR494 loaded with 5.0 wt% photoinitiator cured using 356 nm UV irradiance.

As seen in Figures 5.9 and 5.10, decreasing the intensity through the use of neutral density filters causes deviations in the renormalized data from the unfiltered data to increase. Although the unfiltered, ND01, and ND03 curves do not entirely collapse, the margins of error in the data do overlap. The ND10 data, however, do not overlap with the unfiltered and are not within the margin of error. According to the Figures 5.9 and 5.10, the threshold model becomes increasingly inaccurate as the intensity of UV irradiation is decreased by overcompensating for lower intensities. One explanation for this may be that at low intensities the propagation step, shown in Equation 2.15, is less inhibited by diffusion, which is not accounted for by threshold model.

Inspection of Figures 5.9 and 5.10 also suggest that the critical energy threshold model becomes progressively more inaccurate with increasing UV penetration depth. At a depth of approximately 75 μm, the normalized data for ND01 and ND03 begin to increasingly deviate from the unfiltered data for both 248 nm and 356 nm UV irradiance. This may also be a result of diffusion limited propagation. Figures 5.9 and 5.10 ultimately illustrate that the critical energy threshold model is not robust enough to empirically model the photopolymerization process under low intensity or in thick samples. The primary reason the model breaks down under these conditions is that it fails to fully consider the reaction kinetics of photopolymerization shown in Equations 2.13-2.22.

5.4 Kinetic Effects

The kinetics of free-radical photo-induced polymerizations are dependent on several factors such as the functionality of the monomer and the intensity of UV irradiation; therefore, models that incorporate kinetics to theoretically predict photopolymerization are difficult to develop. Modeling the kinetics of free-radical polymerizations is further complicated by concentrations of inhibitor and initiator, as well as inhibition of oxygen.

5.4.1 Concentration of Inhibitor

Polymerization inhibitors, such as hydroquinone (HQ) and hydroquinone monomethyl ether (MEHQ), are used to promote process and shelf stability of highly reactive acrylate monomer formulations. As illustrated in Equations 2.20-2.22, inhibitors are able to scavenge free-radicals that form during manufacturing or storage of the photoresin formulation. Since the majority of commercially used monomers contain only minute amounts, the effects of inhibitors on cure rate are considered negligible. To better understand the effects of inhibition, a small amount of SR494 was purposely deinhibited and loaded with 5.0 wt.% photoinitiator. The sample was then prepared with different concentrations of MEHQ and cured under 356 nm UV irradiance. The gelation times at a fixed UV penetration depth of 60 μm are shown in Figure 5.11.

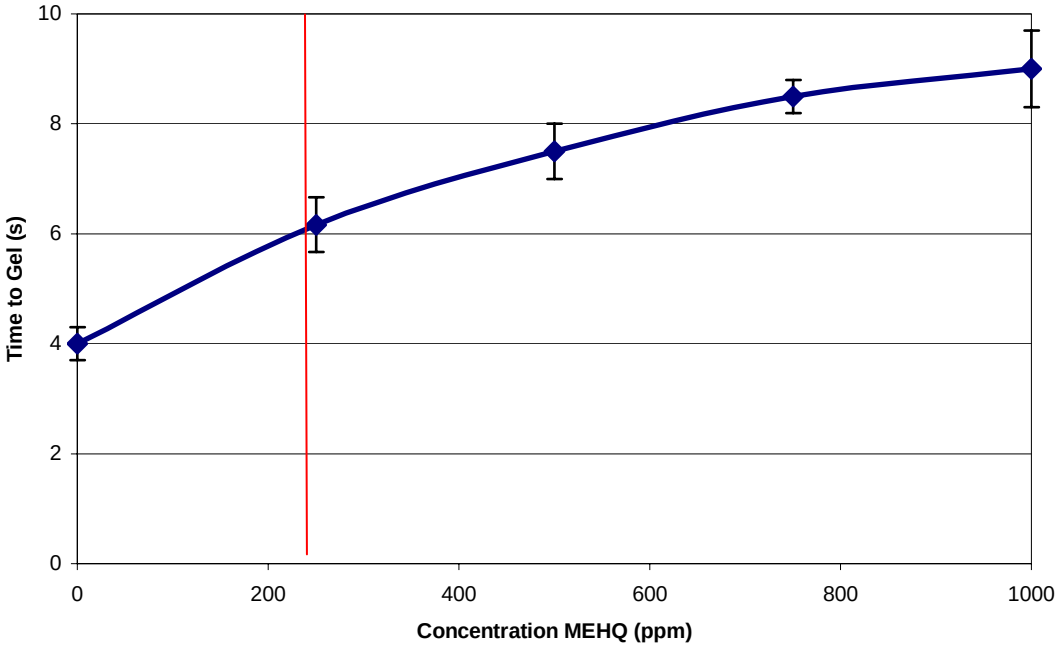

Figure 5.11: Plot of gelation time as a function of inhibitor (MEHQ) concentration for SR494 loaded with 5.0 wt% photoinitiator cured using 356 nm UV irradiance. The vertical line indicates the concentration of inhibitor in the sample as received (240 ppm MEHQ).

As can be seen in Figure 5.11, increasing the concentration of MEHQ lengthens the overall cure time. The addition of MEHQ mainly affects the initiation and propagation steps of the reaction kinetics, shown in Equations 2.13-2.15, by quenching both free and chain radicals before they have a chance to react with other unsaturated sites. MEHQ reacts with chain radicals by hydride abstraction to form a hydroquinone radical that is considered stable and unable to initiate further polymerization. Although the stabilized MEHQ radical cannot initiate polymerization, it can react with additional chain radicals and terminate propagation. Eventually, once all the MEHQ is consumed, the photopolymerization will proceed to gelation. In view of this it is easy to see why the cure time more than doubles for a 1000 ppm increase in MEHQ concentration as shown in Figure 5.11.

In addition, the data in Figure 5.11 demonstrates that the effect of inhibitor on cure time begins to level off around a MEHQ concentration of 750 ppm. Increasing the concentration of inhibitor beyond this point has a less significant effect on the gelation time compared to initial increases in inhibitor concentration. Studies performed to determine the optimal inhibitor concentration necessary to protect commercial formulations from early gelation support the results obtained in this research. In one such investigation[51], Sartomer Inc. used a UV equipped rheometer to determine the effects of varying the concentration of MEHQ in samples of SR351 on cure time. The results of that study agree with the data obtained using microrheology, showing that increasing the concentration of inhibitor will increase the time required to cure the monomer. A 50% increase in gelation time was observed between the 0 ppm and 1000 ppm samples of SR351. The Sartomer results indicate a plateau in cure time was reached around a concentration of 500 ppm MEHQ[51].

5.4.2 Concentration of Photoinitiator and Oxygen Inhibition

Photoinitiator concentration governs both the rate of initiation and the penetration of the incident light into the sample; therefore, it plays an influential role in the photopolymerization process. In theory, one could increase the cure speed by simply increasing the amount of photoinitiator; however, there are limitations and trade-offs such as decreased UV penetration and increased raw material cost. Typically, commercial formulations are loaded with 2.0 to 4.0 wt.% photoinitiator; however, this number varies depending on the structure of photoresin. To understand the curing speed dependence on photoinitiator concentration, different concentrations of photoinitiator (Ciba Irgacure

651) were added to SR494. The system was cured using 356 nm UV illumination at a standard location of 60 μm from the illuminated surface. Figure 5.12 provides data for the cure times for SR494 over a wide range of photoinitiator concentrations. The gelation data is offered in three different scales: 5.12A is plotted on a linear scale, 5.12B a semi-logarithmic scale, and 5.12C a double logarithmic scale.

A.

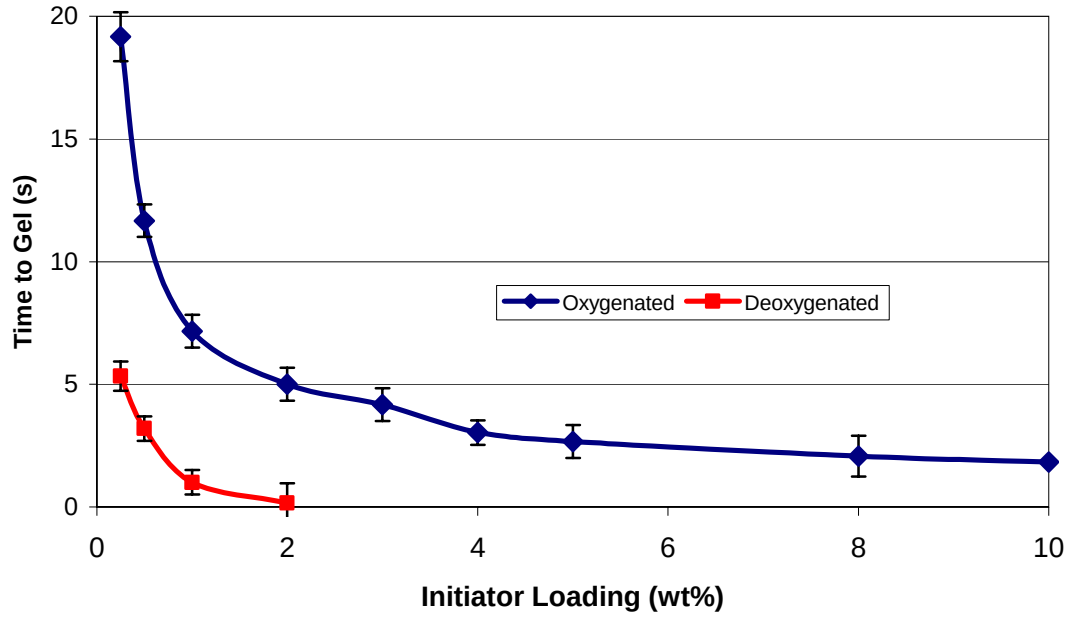

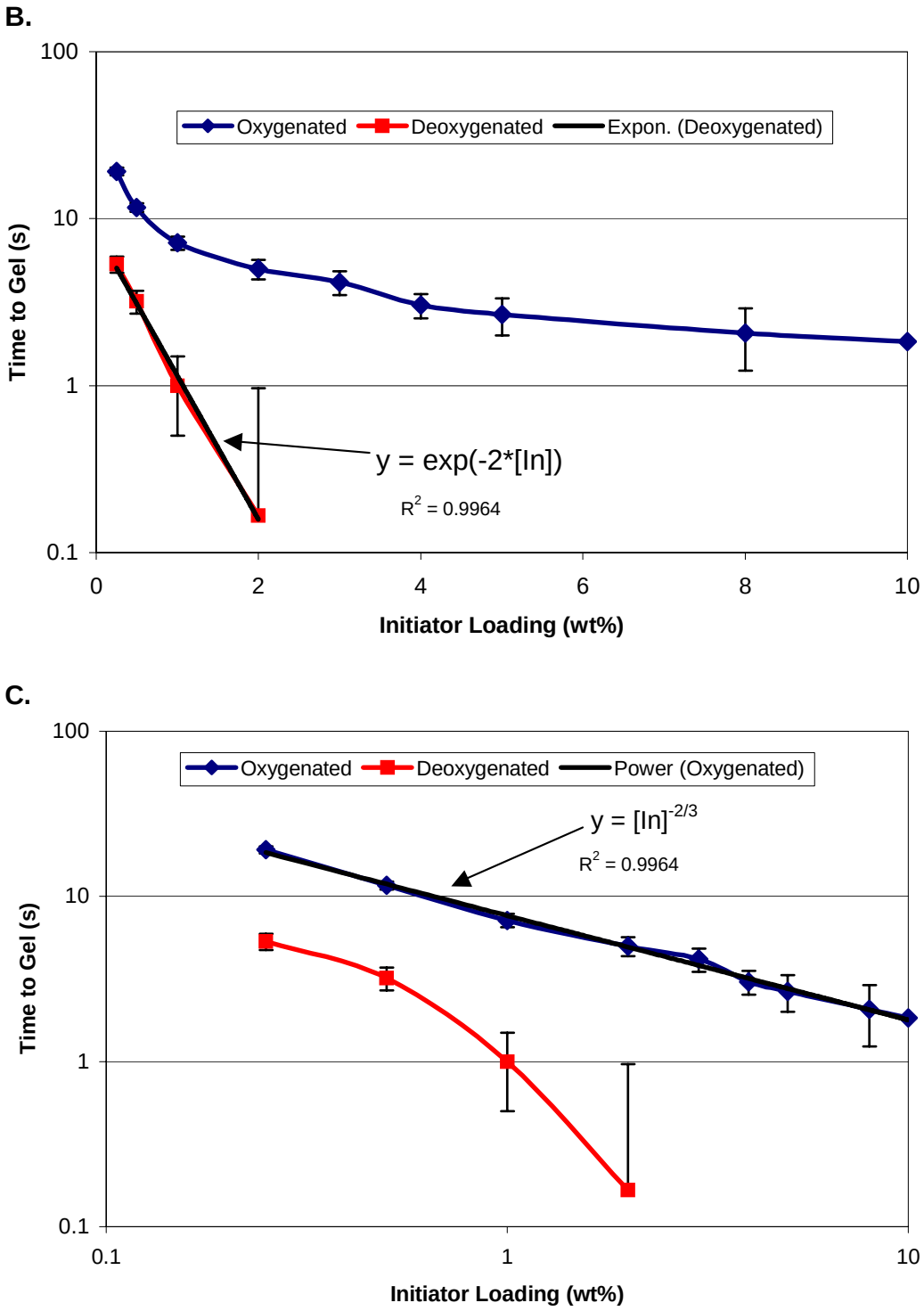

Figure 5.12: Plot of gelation time as a function of initiator (Irgacure 651) loading concentration for both oxygenated and degassed samples of SR494 cured using 356 nm UV irradiance. Plotted in: A: a linear, B: log-linear, and C: double logarithmic scale.

As shown in Figure 5.12A, the gelation time appears to have an exponential dependence on the concentration of initiator; however, Figures 5.12B and 5.12C show that the oxygenated data does not follow an exponential decay, but rather a power-law decay. The fit line for the power law decay is shown in Figures 5.12C. By increasing the amount of photoinitiator, the production of free-radicals by the initiation step, shown as Equations 2.13 and 2.14 in the list of kinetic reactions, is amplified. The increased production of free-radicals leads to the intensification of chain propagation, Equation 2.15, which results in an overall increase in reactivity. Figure 5.12A shows that dependence of gelation time on the concentration of initiator begins to level off around 5.0 wt.%. One explanation for this would be that as the photoinitiator concentration is raised, the penetration depth of the photons decreases according to Beer's law; therefore, a limit exist where increasing the concentration of photoinitiator no longer significantly shortens the gel time.

The results of the initiator loading investigation are supported by studies performed by Rueggeberg *et al.*[52, 53] and Brady *et al.*[54], which use differential photo-calorimetry to determine the effects of initiator concentration on photo-curing of methacrylate dental composites. Both research groups found that higher concentrations of photoinitiator increased both the rate of photopolymerization and the final conversion. An increased rate of polymerization would ultimately lead to a faster cure time as shown in Figures 5.12A-5.12C. Rueggeberg and co-workers, however, went on to observe that the benefits of increasing the concentration of initiator are limited by the absorption and penetration of UV light[52, 53].

Oxygen inhibition negatively impacts the UV curing of acrylate systems by increasing the cure time. Since atmospheric oxygen scavenges active free-radicals, the effects of oxygen inhibition are frequently overcome in industry by increasing the amount of photoinitiator. This approach, however, is usually used in combination with an increase in UV intensity or the addition of oxygen scavengers, because the benefits of simply increasing the concentration of initiator can be insufficient as shown in Figure 5.12A. To better understand the effect of oxygen inhibition on gel time, samples of SR494 were loaded with photoinitiator concentrations ranging from 0.25 wt.% to 2.0 wt.%. The samples were then degassed under vacuum and loaded in the sample chamber in an oxygen-free environment. The system was then cured at the maximum UV illumination intensity in the same fashion as was used in the initiator loading study. The results are exemplified in red in Figures 5.12A-5.12C.

A significant decrease in gelation time was observed for the degassed samples. As seen in Figure 5.12A, the degassed data showed a similar trend to what was observed in the oxygenated samples. Figure 5.12B, however, shows that the degassed data follows an exponential decay, unlike the oxygenated data. Oxygen quenches the free-radicals produced in the initiation step and chain free-radicals, thereby, decreasing the rate of propagating while increasing the rate of termination. As seen in Figure 5.12, the effects of oxygen inhibition are greater at lower concentrations of photoinitiator. Under these conditions, a smaller amount of free-radicals will be generated, resulting in a decreased ability to overcome oxygen inhibition because there are not enough radicals left to efficiently initiate the photopolymerization process. The effects of oxygen are more significant than MEHQ or HQ; unlike polymerization inhibitors, which are used in

limited amounts, oxygen is always present in a system exposed to the atmosphere. As a result, for polymerization to proceed in the presence of oxygen, the number of free-radicals produced via the initiation step shown in Equations 2.13 and 2.14, must be greater than the number of oxygen diradicals present.

Decker *et al.*[28, 29] studied the influence of oxygen on the curing of polyurethane-acrylate resin using carbon dioxide inerting and FTIR. The results of their study support the findings of this research by showing that carbon dioxide inerting significantly increased the cure speed of the resin. In addition, Decker and co-workers found that oxygen inhibition is strongly dependent on the viscosity, temperature, and thickness of the sample[28]. For our investigation, SR494, the resin with the highest viscosity, was used in order to limit the diffusion of oxygen back into the degassed sample. The temperature dependence of oxygen diffusion observed by Decker *et al.* is not expected to significantly contribute to the results obtained in this research since the temperature is expected to remain constant across the 100 micron thin SR494 sample.

CHAPTER 6

CONCLUSIONS AND RECOMMENDATIONS

In this chapter, important results of the research project will be summarized and conclusions will be drawn. Recommendations on how to use the obtained experimental results and how to improve the current experimental setup will be presented. Finally, future research in the utilization of microrheology to study photopolymerization will be proposed.

6.1 Summary

- Limitations of free-radical photopolymerization are mainly a result of an overall lack of understanding of the photopolymerization process.
- Microrheology has the ability to track rheological changes in photoresins with high resolution as a function of both time and location; and therefore, can provide a better understand of the overall process.
- Significant variations in the gelation time were observed as a function of UV penetration depth.
- The energy threshold model fails to accurately predict the gelation time at low intensities and in thick samples.

- The addition of MEHQ decreases the cure speed, but the effect begins to plateau at higher concentrations.

- The effect of initiator concentration on gelation time appears to follow a power law scaling.

- When combined with deoxygenation, the effect of initiator concentration on gelation time appears to follow an exponential scaling.

- Microrheology can be used to optimize formulations and to strengthen and validate models used to predict photopolymerization.

6.2 Conclusions

Despite the widespread use of photopolymerization in numerous industrial applications, limitations that result from a general lack of understanding about the process continue to exist. Specifically, spatial variations of photopolymerization impose significant limitations on applications that require high spatial resolution. Past studies of photo-induced polymerization have been performed using spectroscopy, calorimetry, and rheology. Although preceding research has expanded the knowledge of the photopolymerization process, the techniques used in these studies lack the ability to monitor photopolymerization with both high spatial and temporal resolution.

To address these issues, the emerging technique of microrheology was employed to study and perform in-situ monitoring of the photopolymerization process. The initial results prove the ability of microrheology to track rheological changes in samples of photoresins as a function of both time and location. Through this research, a better

understanding of both the kinetic behavior and spatial variations of acrylate photoresins is achieved.

A significant increase in the gelation time was observed as a function of UV penetration depth. The trend was found to be independent of monomer functionality and UV intensity. These results show that microrheology has the potential to provide considerable insight into the spatial inhomogeneities that plague many applications. The results of the intensity study not only show that decreasing the UV intensity decreases the gelation time, but also that the simple energy threshold model is not accurate at empirically predicting photopolymerization at low intensities of UV irradiation or in deep samples. The intensity study also provides insight into the rate constant of the initiation mechanism.

The relationships observed in Figures 5.11 and 5.12A of the kinetics section of the results are highly important for optimizing commercial photoresin formulations. Formulators often add excessive amounts of inhibitors to a monomer with the expectation of obtaining an extended shelf life. Figure 5.11, however, shows that an optimal concentration of inhibitor exists where the photoresin is both protected from early polymerization yet maintains an acceptable cure speed. Figure 5.11 also provides a good understanding of the rate constant of inhibition. Figure 5.12A shows that adding excessive amounts of photoinitiator only increases cure rate to a certain extent. Photoinitiator is considered the most expensive component of the photoresin system; therefore, determining the minimum concentration of photoinitiator necessary to achieve a maximum rate of initiation would greatly reduce material costs. Using microrheology,

the optimal value of inhibitor and initiator concentration can be determined for nearly any photoresin.

In addition, the experimental data can be used to validate and strengthen models that are currently being developed to predict the outcome of photopolymerization. The results give a good understanding of how the reaction kinetics, shown in Equations 2.13-2.22, are affected by changing system parameters. This information could be used to test the predictive powers of current models and aid in the development of new models. For instance, it is expected that the data in Figures 5.12A-5.12C could be used to develop an accurate model that is able to balance the initially dominant initiation and inhibition (oxygen and polymerization inhibition) kinetics and the propagation and termination kinetics that determine the later stage of the process.

In conclusion, microrheology is an effective tool for monitoring the photopolymerization process. The research offered in this thesis uniquely expands the understanding of photo-induced free-radical polymerization. Microrheology allows for the optimization of process formulations and provides important kinetic information that could be used to advance modeling efforts. The presented research achieves the goals set forth by the objective and gives the basis and direction for future work.

6.3 Recommendations

The designed experimental setup is robust and yields reproducible results; however, there is potential for improvement. The majority of error in the data is a result of using a primitive shutter, a simple iris diaphragm, to control the exposure of the sample to UV light. At best, the exact moment at which the iris diaphragm is fully

opened can be determined to within half a second. Adding an electronically controlled high-speed shutter to the current setup would improve control of the UV light path and eliminate this source of error. A high-speed shutter would also allow for the accurate variation of illumination profile as a function of time. Using an electronically-timed shutter, sequences of light and dark of UV illumination periods could be delivered to the sample.

Another fundamental source of error in this research was the loss of resolution associated with the photobleaching of the embedded silica particles. Photobleaching made images difficult to analyze toward the end of the experiment and resulted in artifacts for some data sets. In addition, the high density silica particles sedimented relatively quickly and aggregated at the bottom of the sample chamber, especially for low-viscosity monomers. As a result, fewer particles were available for statistical analysis and the contrast and clarity of the images were reduced. Using less dense, more fluorescently stable particles, such as commercial produced polystyrene particles, would greatly reduce error in the image analysis. Polystyrene particles, however, swell and leach fluorescence in the current system of acrylate monomers. As a result, alternative methods like growing a thin silica layer on a polystyrene particle need to be investigated.

The experimental data obtained from this research has the potential to positively impact efforts to model and control the process of photopolymerization. The empirical threshold model is the least complicated model applied to photopolymerization. The model is based on the idea that polymerization reaches percolation after a certain amount of critical energy is delivered to the sample. The model neglects to consider the kinetics of free-radical polymerization, listed by Equations 2.13-2.22, and the heat and mass

transfer associated with photo-induced polymerizations. Consequently, the simplicity of the model is lost in the fact that new values of the energy threshold must be determined for each experimental formulation and geometry. Subsequent models have been developed that incorporate both reaction kinetics and transport processes. The data ascertained in this research could be used to strengthen and validate current and future models.

6.4 Future Research

The results obtained in this study show that the current experimental system is capable of monitoring free-radical photopolymerization in acrylates, which is of importance to applications like coatings and stereolithography. The next and simplest step would be to use the current setup to test water based systems such as photosensitive hydrogels. These materials form cross-linked hydrophilic polymer networks that are used in applications like contact lenses and drug delivery. It is expected that results similar to those obtained for acrylate systems could be ascertained for hydrogels. One benefit of using hydrogel instead of acrylates is that hydrogels would allow the use of commercial available polystyrene particles, which have the potential of enhancing the quality of data. If microrheology is found to be capable of studying these systems the potential exist to use microrheology as a tool for quality control and high-throughput screening of industrial formulations.

The groundwork has been established and preliminary results proving the ability of microrheology to monitor the photo-induced polymerization of hydrogels have been obtained. Further research must be performed, and thus the results are not presented in

this work. It is anticipated that current predictive models that incorporate reaction kinetics and transport processes for acrylate stereolithography resins could be comprehensive enough to describe the fundamental aspects of hydrogel polymerization. The experimental data expected to be obtained from the above proposed research could potentially be used to strengthen current models and simplify the development of new models for photo-induced hydrogel polymerization.

The variation of illumination profile as a function of time and space is another interesting future research objective. As illustrated in Figure 6.1, a patterned lithographic mask with micrometer-sized line spacings will be used in conjunction with videomicroscopy to study spatial effects. The masking experiments are expected to enable quantitative characterization of shrinkage effects during photopolymerization and provide three-dimensional profiles of gelation. The current setup utilizes a mask with a single millimeter-sized gap, which is sufficient to minimize the effects of shrinkage, but not to study the process of shrinkage quantitatively. In addition, high-speed shutters could be used to study temporal effects by controlling sequences of light and dark periods of UV illumination, as shown in Figure 6.2. These experiments are expected to yield data that can be used to characterize the rate of reaction that proceeds after UV irradiation has been terminated. Additionally, the temporal study will be used to characterize the effects of varying UV illumination on the critical energy threshold required for polymerization to proceed to completion.

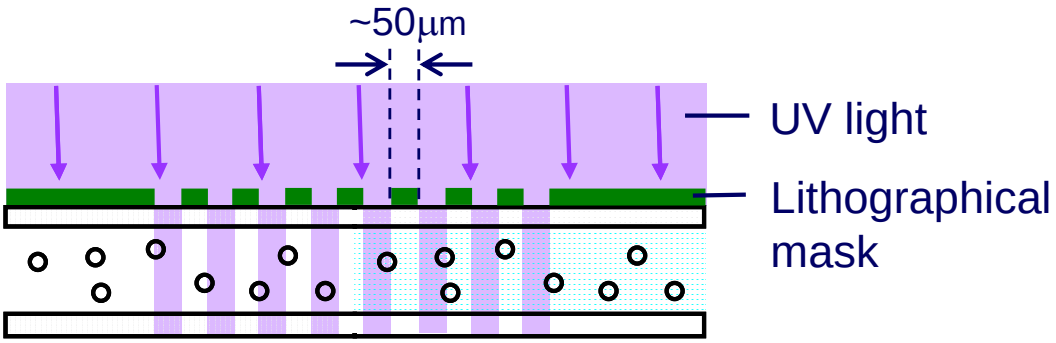

***Figure 6.1:** Experimental design for spatial patterned photo-masks.*

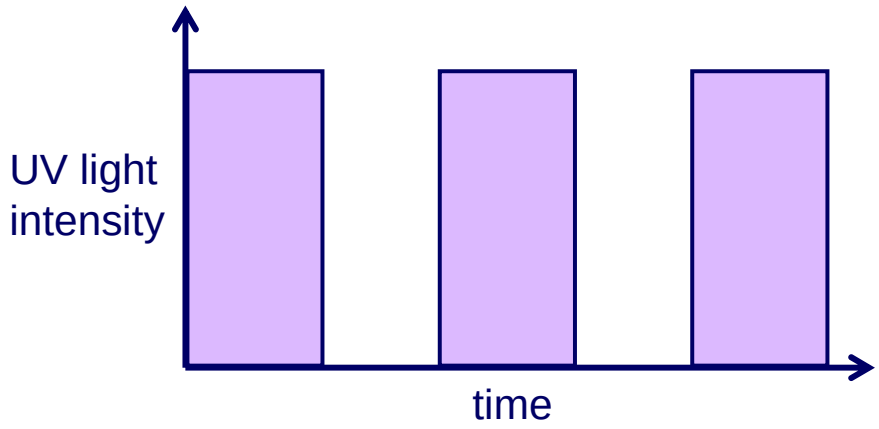

***Figure 6.2:** Temporal modulation of illumination profile using electronic shutters.*

The ultimate future goal would be the commercial implementation of microrheology as a tool for high-throughput screening and in-line quality control monitoring. The ability to use microrheology to perform high-throughput screening has already been well-established and the results obtained in this work prove that microrheology has the ability to accurately perform in-situ process monitoring. The current experimental setup which uses videomicroscopy is almost certainly too slow and lacks the desired spatial resolution required for screening and in-line quality monitoring; therefore, different microrheological techniques need to be investigated. DWS, a multiple scattering technique that can detect particle displacements at the sub-nanometer

level, has the greatest potential for commercial implementation as a real-time technique. The implementation of microrheology in commercial processes has the potential to improve product quality and uniformity, as well as lower process cost associated with manual quality control.

REFERENCES

1. Fouassier, J. P. and J. F. Rabek. Radiation Curing in Polymer Science and Technology Volume III: Polymerizations Mechanisms. London: Elsevier Applied Science, 1993.

2. Drobny, J. G. Radiation Technology for Polymers. London: CRC Press, 2003.

3. Roffey, C. G. Photopolymerization of Surface Coatings. New York: John Wiley & Sons, 1982.

4. Pappas, S. P. UV Curing: Science & Technology Volume II. Norwalk, CT: Technology Marketing Corporation, 1985.

5. Decker, C. "Photoinitiated Curing of Multifunctional Monomers." Acta Polymer 43 (1994): 333-347.

6. Kaur, M. and Srivastava, A. K. "Photopolymerization: A Review." Journal of Macromolecule Science- Polymer Reviews 4 (2002): 481-512.

7. Decker, C. and Moussa, K. "A New Method for Monitoring Ultra-Fast Photopolymerizations By Real-Time Infrared Spectroscopy (RTIR)" Makrol Chem 189 (1988): 2318-2394.

8. Clark, S., Hoyle, C., Jonsson, S., Morel, F., and Decker, C. "Photopolymerization of acrylates using N-aliphaticmaleimides as photoinitiators." Polymer 40 (1999): 5063-5072.

9. Dias, A., and Moreira, R. "New Technologies in Real-Time Infrared Spectroscopy (RTIR)." Surface Coatings International 8: (2000): 382.

10. Lin, Y. and Stansbury, J. "Application of FT-NIR spectroscopy for monitoring the kinetics of photoinitiated methacrylate/vinyl ether copolymerizations." Journal of the American Chemical Society 42 (2001): 809.

11. Nelson, E. and Scranton, A. "In situ Raman spectroscopy for cure monitoring of cationic photopolymerizations of divinyl ethers." Journal of Raman Spectroscopy (1996): 413.

12. Carlini, C., Ciardelli, F., Rolla, P., *et al.* "Kinetic-Analysis of Photoinitiated Polymerization of N-Butyl Acrylate up to High Conversion by Microwave

Dielectrometry." Journal of Polymer Science Part B—Polymer Physics 27 (1989): 189-197.

13. Carlini, C., Rolla, P. and Tombari, E. "Measurement Method and Apparatus for Monitoring the Kinetics of Polymerization and Cross-Linking Reactions by Microwave Dielectrometry." Journal of Applied Polymer Science 41 (1990): 805-818.

14. Nakamuchi, T. "Time-Resolved Measurements of Mechanical Properties Using a Rheological Apparatus" Progress in Organic Coatings 14 (1986): 23.

15. Watanbe, K. "Rheological Studies of Ultraviolet Curing with an Oscillating Plate Rheometer." Journal of Applied Polymer Science 29 (1986): 323-332.

16. Davison, J. and Guthrie, J. "Photochemorheological Studies of UV Curing Processes." JOCCA Surface Coatings International 75 (1992): 315-322.

17. Chiou, B., English, R. and Khan, S. "Rheology and Photo-Cross-Linking of Thiol-ene Polymers." Macromolecules 29 (1996): 5368-5374.

18. Chiou, B., English, R. and Khan, S. "Real-Time and in-situ Rheological Studies on the UV Curing Kinetics of Thiol-ene Polymers." Macromolecules 30 (1997): 7322-7328.

19. Scherzer, T. "Real-Time FTIR-ATR Spectroscopy of Photopolymerization Reactions." Macromolecule Symposium 184 (2002): 79-97.

20. Dietz, J., Elliott, B. and Peppas, N. "Real-Time Attenuated Total Reflectance—Fourier Transform Infrared Spectroscopy to Monitor Multiacrylate Polymerization Reactions." Macromolecules 28 (1995): 5163-5166.

21. Lange, J. "Viscoelastic Properties and Transitions during Thermal and UV Cure of a Methacrylate Resin." Polymer Engineering and Science 39 (1999): 1651-1660.

22. Naghash, H., Okay, O. and Yagci, Y. "Gel Formation by Chain-Crosslinking Photopolymerization of Methyl Methacrylate and Ethylene Glycol Dimethacrylate." Polymer 38 (1997): 1187-1196.

23. Claesson, H., Malmstrom, E., Johansson, M., *et al.* "Rheological Behavior During UV-Curing of a Star-Branched Polyester." Progress in Organic Coatings 44 (2002): 63-67.

24. Botella, A., Dupuy, J., Roche, A., *et al.* "Photo-Rheometry/NIR Spectrometry: An in-situ Technique for Monitoring Conversion and Viscoelastic Properties During

Photopolymerization." Macromolecule Rapid Communication 25 (2004): 1155-1158.

25. Lee, J., Prud'homme R. and Aksay, I. "Cure Depth in Photopolymerization: Experiments and Theory." Journal of Materials Research 16 (2001): 3536-3544.

26. Halley, P. "Chemorheology of Thermosets—An Overview." Polymer Engineering and Science 36 (1996): 593-608.

27. Koleske, J. Radiation Curing of Coatings. New York: John Wiley & Sons, 1982.

28. Studer, K., Decker, C., Beck, E., et *al.* "Overcoming Oxygen Inhibition in UV-Curing of Acrylate Coatings by Carbon Dioxide Inerting, Part I." Progress in Organic Coatings 48 (2003): 92-100.

29. Studer, K., Decker, C., Beck, E., *et al.* "Overcoming Oxygen Inhibition in UV-Curing of Acrylate Coatings by Carbon Dioxide Inerting, Part II." Progress in Organic Coatings 48 (2003): 101-111.

30. Winter, H. H. and Chambon, F. "Analysis of Linear Viscoelasticity of a Crosslinking Polymer at the Gel Point." Journal of Rheology 30 (1986): 367-382.

31. Pizzi A. "Extension of Simple Polycondensation Gelation Theories to Simple Radical and Mixed Polycondensation/Radical Gelation." Journal of Applied Polymer Science 71 (1999) 517-521.

32. Flory, J. P. Principles of Polymer Chemistry. Ithaca, NY: Cornell University Press, 1953.

33. Winter, H. H. and Mours, M. "Rheology of Polymers Near Liquid-Solid Transitions." Advances in Polymer Science 134 (1997): 1-70.

34. Barachevsky, V. "Applied Aspects of Organic Photochemistry." High Energy Chemistry 37 (2003): 6-16.

35. Santler, G., Schultes, G., Gaggl A., *et al.* "Stereolithography Versus Milled Three-Dimensional Models: Comparison of Production Method, Indication, and Accuracy." Computer Aided Surgery 3 (1998): 248-256.

36. Gardel, M. L., *et al.* "Microrheology." Department of Physics and Division of Engineering and Applied Sciences, Harvard University, Cambridge MA: 1-55.

37. Waigh, T. A. "Microrheology of Complex Fluids." Reports on Progress in Physics 68 (2005): 685-742.

38. Breedveld, V. and Pine, D. "Microrheology as a Tool for High-Throughput Screening." Journal of Materials Science 38 (2003): 4461-4470.

39. Mukhopadhyay, A. and Granick, S. "Micro-and Nanorheology." Current Opinion in Colloid & Interface Science 6 (2001): 423-429.

40. Puskas, J. In-situ Spectroscopy of Monomer and Polymer Synthesis. New York: Kluwer Academic/Plenum Publishers, 2003.

41. Alfassi, Z. B. General Aspects of the Chemistry of Radicals. Chichester, New York: Wiley, 1999.

42. Bower, D. L. and W. F. Maddams. The Vibrational Spectroscopy of Polymers. Cambridge, New York: Cambridge University Press, 1989.

43. Gallagher, P. K. Handbook of Thermal Analysis and Calorimetry. New York: Elsevier, 1998.

44. Liebman, J. L. Energetics of Organic Free Radicals. London, UK: Blackie Academic & Professional, 1996.

45. Murayama, T. Dynamic Mechanical Analysis of Polymeric Material. New York: Elsevier Scientific, 1978.

46. Tolpekin, V., Duits, M., van den Ende, D. *et al.* "Stability Ratio in Binary Hard Sphere Suspensions, Measured via Time-Resolved Microscopy." Langmuir 19 (2003): 4127-4137.

47. Breedveld, V. Tutorial for OpenBox and IDL: Particle Tracking and Microrheology. Georgia Institute of Technology, May 2005.

48. Otsubo, Y., Amari, T., and Watanabe, K. "Rheological Behavior of Epoxy Acrylate Prepolymer during UV Curing." Journal of Applied Polymer Science 29 (1984): 4071-4080.

49. Otsubo, Y., Amari, T., and Watanabe, K. "Rheological Measurements of Cure Rate of UV Inks." Journal of Applied Polymer Science 31 (1986): 2099-2108.

50. Lecamp, L., Youssef, B., Bunel C., *et al.* "Photoinitiated Polymerization of a Dimethacrylate Oligomer: Influence of Photoinitiator Concentration, Temperature and Light Intensity." Polymer Papers 38 (1997): 6089-6096.

51. Sartomer Company. "Inhibition of Acrylate UV-Curing Systems." Company Literature (1990): 1-6.

52. Rueggeberg, F., Ergle, J. and Lockwood, P. “Effect of Photoinitiator Level on Properties of a Light-Cured and Post-Cure Heated Model Resin System.” Dental Materials 13 (1997): 360-364.

53. Whitters, C., Strang, R., Brown, D., *et al.* “Dental Materials: 1997 Literature Review.” Journal of Dentistry 27 (1999): 401–435.

54. Brady, G. and Holloran, J. “Differential photo-calorimetry of photopolymerizable ceramic suspensions.” Journal of Materials Science 33 (1998): 4551 – 4560.